ROCK CUTTING THEORY FOR PDC CUTTERS

by

VEERAMANI PRAKASH

B.E(HONORS)., Madras University, India, 1980

A MASTER'S THESIS

submitted in partial fulfillment of the
requirements for the degree

MASTER OF SCIENCE

Department of Mechanical Engineering

Kansas State University
Manhattan, Kansas

1982

Approved by:

F. C. Appl
Major Professor

TABLE OF CONTENTS

TABLE OF CONTENTS - Continued

LIST OF TABLES

LIST OF FIGURES

LIST OF FIGURES - Continued

NOMENCLATURE

α	**Rake** Angle
ϕ	Angle of the 'shear plane'
t	Depth of cut
σ_b	Borehole pressure
σ_{p1}, σ_{p2}	Pore pressure
σ_n	Normal stress on the 'shear plane'
τ_n	Shear stress on the 'shear plane'
σ_t	Normal stress on the rake face
τ_t	Shear stress on the rake face
V	Velocity of the cutter
V_c	Velocity of the chip
V^*	Velocity discontinuity
F_t	Tangential cutting force
F_n	Normal cutting force
AB	Shear plane
BC	Rake face
CA	Plane at an angle θ from the 'shear plane'
θ	Angle between CA and AB
a_1, a_2, a_3	Areas along the planes AB, BC & CA
ν	Rock porosity
μ	Friction factor
τ	Shear stress along the Mohr's envelope

σ	Normal stress along the Mohr's envelope
τ_∞	Shear stress at infinity along the Mohr's envelope
ψ, b	Parameters in the envelope equation
$F_1(V^*)$, $F_2(V_c)$	Velocity effects
σ_x, σ_y, τ_{xy}	Stresses in the basic stress element
p	Hydrostatic pressure
k	Yield shear stress
σ_I, τ_I	Stresses on the i line
σ_J, τ_J	Stresses on the j line
γ	Angle in the Mohr's circle
u, v	Velocities along the i and j lines
$\dot{e}_x$, $\dot{e}_y$, $\dot{e}_{xy}$	Strain rates
λ	Constant parameter

1.0 INTRODUCTION

Shale drilling represents about 50% of the oil well footage in the United States [1]. Shale is a term used to describe a rather broad category of rock formations which typically do not have high compressive strength but are highly ductile, especially when subjected to confining pressure.

Toothed roller cone drill bits are used to drill most of the oil well footage, but often these bits do not perform well in shale because ductility impedes chip removal. Within the last few years a new type of diamond cutter (synthetic polycrystalline diamond compact, PDC) has become commercially available and appears to have a great potential for oil well drill bits. A PDC cutter is shown in Figure 3. Several companies are now manufacturing these bits and many designs have emerged. Examples of PDC drill bits are shown in Figures 1, 2 & 4. The design of these bits are different from each other and there is no fundamental design which governs the number of individual cutter edges, their relative placement, bit shape and other parameters which influence the bit performance. Several of these bits have been sucessful in shale. However, bit design and development has been done primarily by empirical analysis and trial and error methods. For continued improvement of these bits there is need for a basic theory of cutting for PDC cutters. This would then be the basis for a drilling theory for PDC oil well drill bits which could be used to develop improved bits.

Some research work has been done on cutting shale with PDC cutters but the experimental results seem somewhat contradicting and the theoretical

FIGURE 1 : A P.D.C. DRILL BIT

FIGURE 2 : A P.D.C. DRILL BIT

FIGURE 3 : A P.D.C. CUTTER

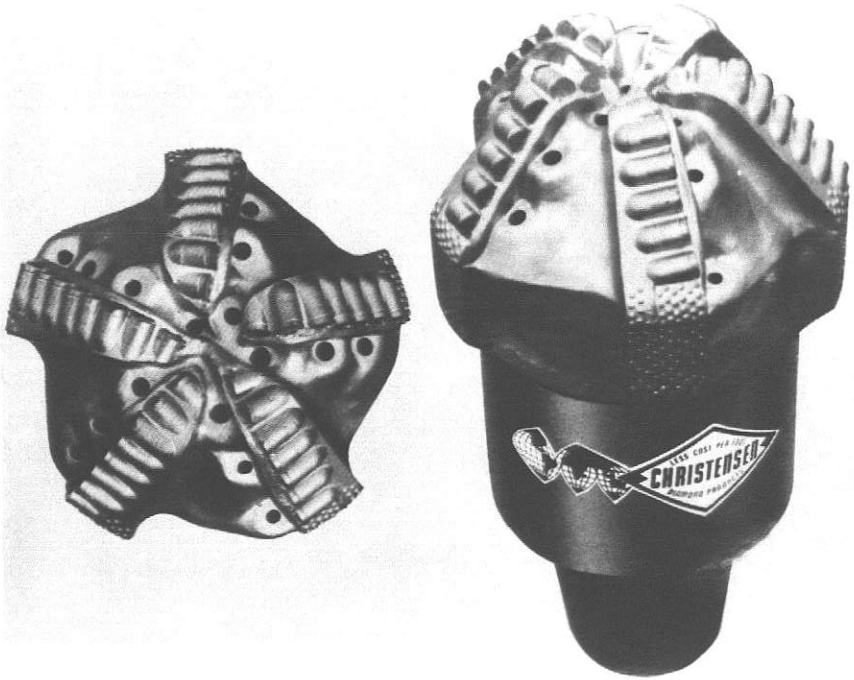

FIGURE 4 : A P.D.C. DRILL BIT

model needs improvement.

J.B. Cheatham and W.H. Daniel [2] have studied the factors influencing the cutting of shale with single PDC cutters by conducting experiments on a shale sample under pressure.

J.A. Salzer and J.F. Melaugh [1] have also performed single cutter experiments with PDC cutters but the results of their experiments do not seem to agree well with Cheatham's experiments. The reasons for the difference are not clearly understood. Furthermore these experiments are very costly.

T.W. Miller and J.B. Cheatham [3] have also developed a simplified cutting theory but it does not satisfactorily explain the behaviour of PDC cutters in drilling shale.

Therefore, the development of a satisfactory cutting theory which can explain the results of the experiments and which can be effectively used to improve the design of drill bits is necessary.

The present study is aimed at developing a viable cutting theory for a single PDC cutter. This work is the first step in the development of a drilling theory for actual multiple PDC cutter drill bits.

A Merchant's type plasticity solution is proposed in this study. The effects of borehole pressure, pore pressure in the rock, cutter velocity and rock properties have been incorporated in the theory.

It is known from the literature [4, 5] that there are two theories of plasticity which have been proposed for materials with strength that varies with mean pressure, and neither of them explains all aspects of the behaviour of such materials. Both the theories will be used in solving the cutting problem and the solutions will be compared.

The rock failure criterion used is the well known Mohr's envelope

which is widely used for engineering analysis of problems involving rock failure.

A first attempt has been made to theoretically model the effect of cutting velocity on the cutting forces. It appears that this is significant because the differences in the results of previous experiments are partially explained by the velocity effect.

The cutting problem is formulated by considering equilibrium, continuity and failure criterion and is solved by a numerical procedure to calculate the cutting forces.

2.0 FORMULATION OF THE CUTTING PROBLEM

2.1 Introduction

The basic cutting problem involves the movement of the single edge cutter in the transverse direction over a stationary rock material to produce a chip. Figure 5 shows the cutting process. Although the actual process is three-dimensional the analysis is done for a two-dimensional flow field. The problem is therefore considered to be a plane strain two-dimensional problem. The tool is rigid and has a straight edge of unit width. The rake angle, α , of the tool which is the angle between the upper face of the tool and the normal to the material surface being cut is considered to be negative as shown. The depth of cut is designated by t, as shown in the Figure. It is assumed that the friction between the rake face of the tool and the chip can be represented by the coefficient μ. The rock material is assumed to be rigid-plastic. The rock is assumed to be a composite material of solid rock and fluid pores. The fluid in the pores exerts a pressure, which affects the cutting process. The effect is not clearly understood and in the present study, it is assumed that there is a variation of the pore pressure from near the 'shear plane' to the surface near the rake face. Referring to the Figure, the pore pressure near the 'shear plane' is σ_{p1} and the pore pressure near the rake face is σ_{p2}.

The whole cutting process takes place at large depths at the bottom of a borehole and the borehole mud exerts a pressure on the chip and the tool. This effect makes the problem different from conventional metal cutting processes. Referring to the Figure, σ_b is the borehole pressure

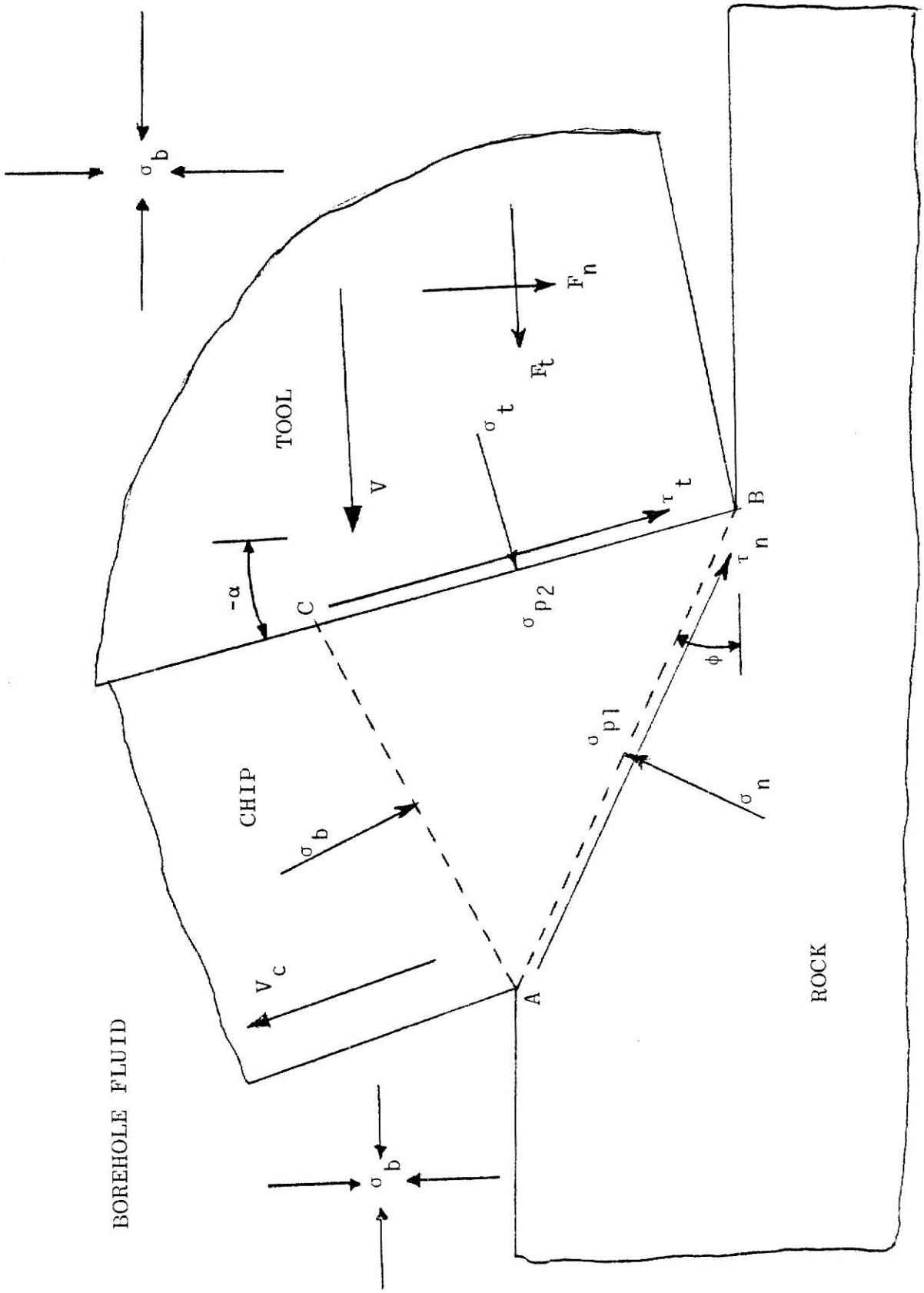

FIGURE 5 : SCHEMATIC REPRESENTATION OF THE CUTTING PROBLEM

assumed to act in a direction perpendicular to the rock surface.

The cutter moves with a velocity V in the direction shown. It is assumed that yielding of the rock material occurs, according to the Von-Mises Yield criterion, along a single plane known as the 'shear plane', designated by the plane AB. Side flow, work hardening and temperature effects are neglected. The angle made by the 'shear plane' with the direction of travel of the cutter is denoted by ϕ. The normal and tangential cutting forces are denoted by F_n and F_t.

2.2 Equilibrium Condition Formulation

Figure 6 shows the various stresses in equilibrium on a rock element which is at yield conditions along the 'shear plane'. The stresses on the rake face BC are the normal stress σ_t and the shear stress τ_t. The borehole pressure σ_b acts on the plane AC perpendicular to the rock surface. On the 'shear plane' AB the stresses are σ_n and τ_n. The planes AB, BC & CA are of unit width and their areas are a_1, a_2 & a_3 respectively.

The areas are given by the following relationships in terms of the angles.

$$a_1 = \frac{t}{\sin(\phi)} \tag{2-1}$$

$$\frac{a_2}{a_1} = \sin(\phi-\alpha) + \tan\left[\theta-(\phi-\alpha)\right]\cos(\phi-\alpha) \tag{2-2}$$

$$\frac{a_3}{a_1} = \frac{\cos(\phi-\alpha)}{\cos\left[\theta-(\phi-\alpha)\right]} \tag{2-3}$$

Figure 7 is a schematic representation of the tool-chip interface.

The surface of the tool is in contact with both solid rock and fluid in the pores.

J.C. Jaeger and N.G.W. Cook [6] and L.L. Karafiath and E.A. Nowatzki [5] have analysed the void areas as a percentage of the total area. Using the same idea and assuming the porosity effect to be $\nu^{2/3}$ (ν is the rock porosity), the effective stress is given by the expression

$$\sigma_t - \nu^{2/3} \sigma_{p2} \tag{2-4}$$

The shear stress on the tool face is given by

$$\tau_t = \mu (\sigma_t - \nu^{2/3} \sigma_{p2}) \tag{2-5}$$

For the rock element shown in Figure 6 to be in equilibrium, the forces and moments must balance. Balancing the forces in the direction parallel to the 'shear plane' gives

$$\tau_n a_1 + \tau_t a_2 \sin(\phi - \alpha) - \sigma_t a_2 \cos(\phi - \alpha) + \sigma_b a_3 \sin(\theta) = 0 \tag{2-6}$$

Balancing the forces in the direction perpendicular to the 'shear plane' yields

$$\sigma_n a_1 - \tau_t a_2 \cos(\phi - \alpha) - \sigma_t a_2 \sin(\phi - \alpha) - \sigma_b a_3 \cos(\theta) = 0 \tag{2-7}$$

Taking clockwise moments about the point D on Figure 6, the following moment equation is obtained.

$$\sigma_b a_3 \left[\frac{a_3}{2} - \frac{a_1}{2} \cos(\theta)\right] - \sigma_t a_2 \left[\frac{a_2}{2} - \frac{a_1}{2} \sin(\phi - \alpha)\right] + \tau_t a_2 \frac{a_1}{2} \cos(\phi - \alpha) = 0 \tag{2-8}$$

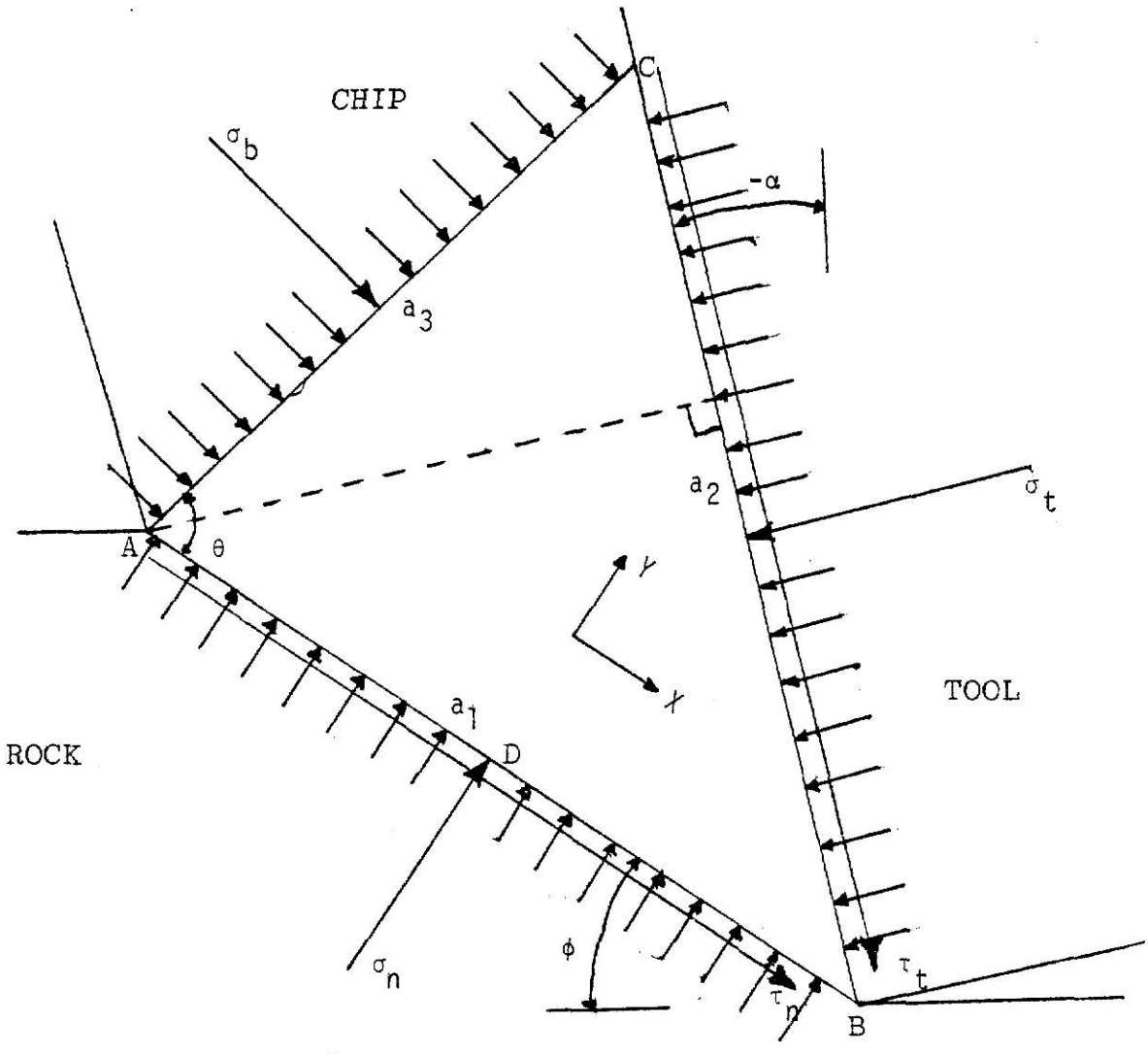

FIGURE 6 : STRESSES IN EQUILIBRIUM ON THE ROCK ELEMENT

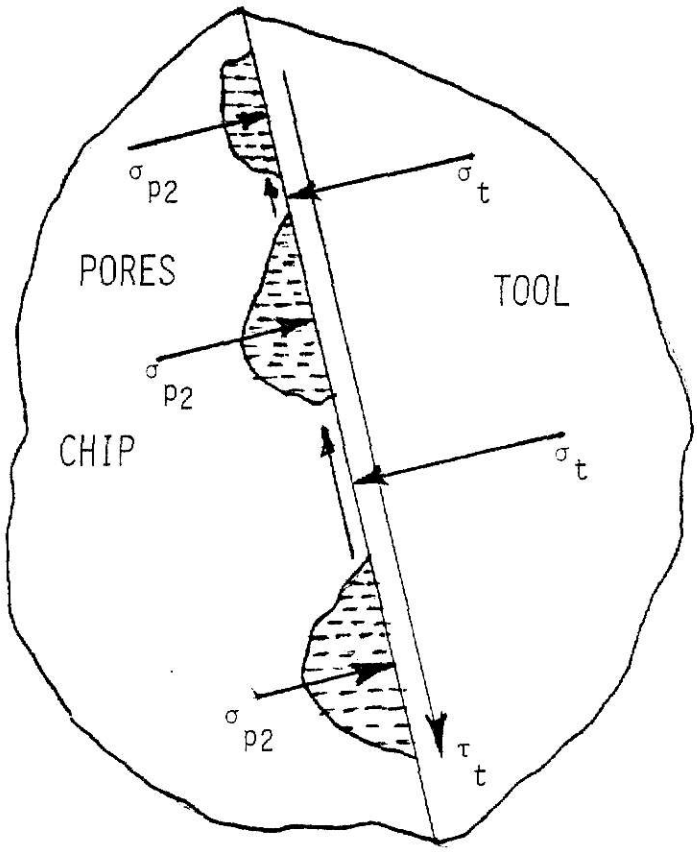

FIGURE 7 : TOOL CHIP INTERFACE

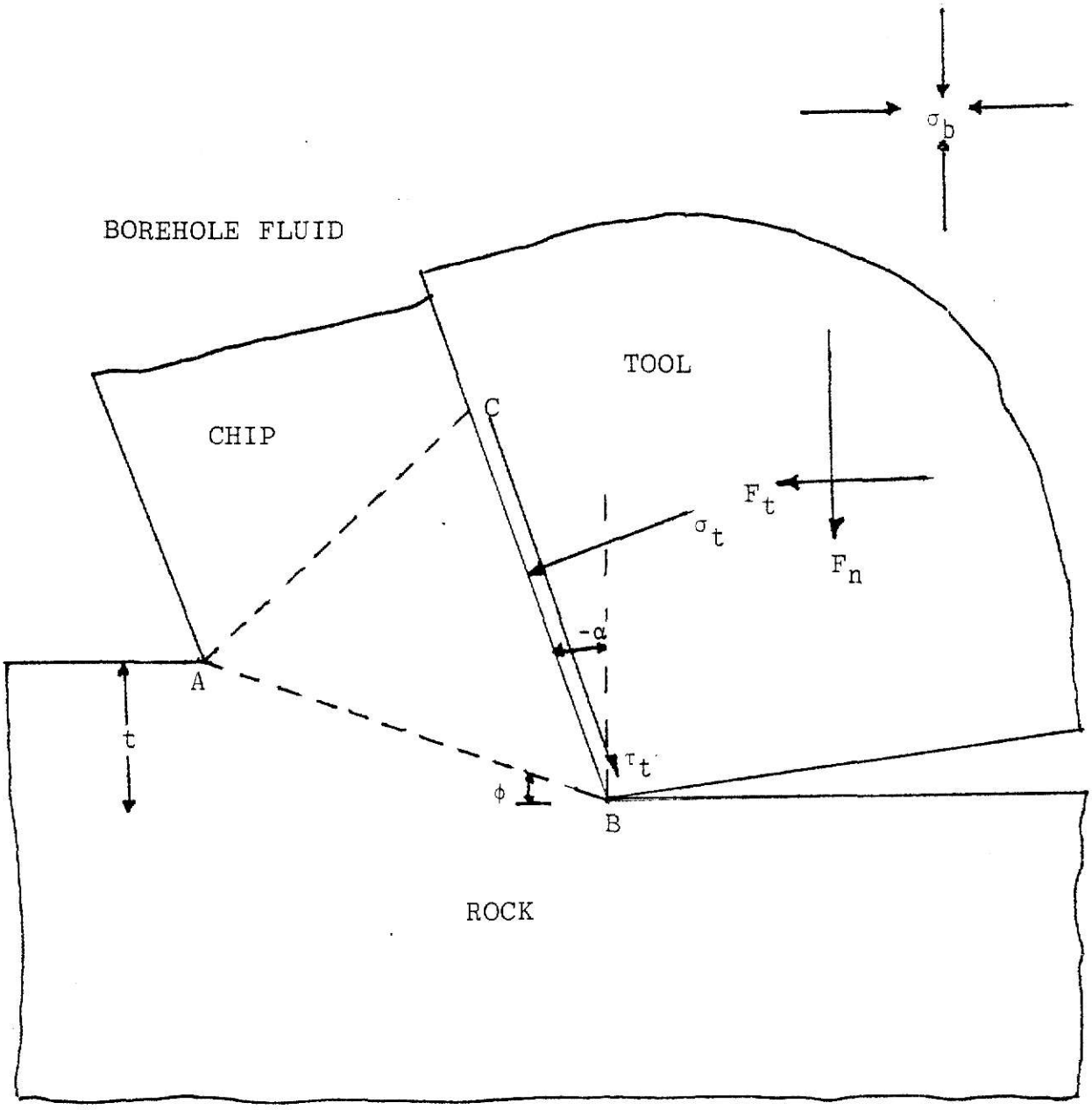

FIGURE 8 : CUTTING FORCE COMPONENTS ON THE TOOL.

Substituting the value of τ_t from (2-5) in (2-8) gives the expression for the normal stress on the rake face as

$$\sigma_t = \frac{\left[\sigma_b \frac{a_3}{a_1}\left[\frac{a_3}{a_1} - \cos(\theta)\right]\right] - \mu\, \nu^{2/3}\, \sigma_{p2}\, \frac{a_2}{a_1} \cos(\phi-\alpha)}{\frac{a_2}{a_1}\left[\frac{a_2}{a_1} - \sin(\phi-\alpha) - \mu \cos(\phi-\alpha)\right]} \qquad (2\text{-}9)$$

The shear stress on the tool is given by the expression (2-5).

2.3 Cutting Forces on the Tool

The cutting forces on the tool are made up of two components; F_t the tangential force in the direction of travel of the cutter; F_n the normal force in the direction perpendicular to the direction of travel of the cutter.

Figure 8 shows the two components of the force. The forces per unit area of cut are given by balancing the stresses shown in the Figure.

$$\frac{F_t}{t} = \left[(\sigma_t - \sigma_b)\cos(\alpha) + \mu\,(\sigma_t - \nu^{2/3}\,\sigma_{p2})\sin(\alpha)\right] \frac{a_2}{a_1} \frac{1}{\sin(\phi)} \qquad (2\text{-}10)$$

$$\frac{F_n}{t} = \left[-(\sigma_t - \sigma_b)\sin(\alpha) + \mu\,(\sigma_t - \nu^{2/3}\,\sigma_{p2})\cos(\alpha)\right] \frac{a_2}{a_1} \frac{1}{\sin(\phi)} \qquad (2\text{-}11)$$

These expressions are used in the computer programs in Appendix I & II to calculate the forces.

3.0 ROCK FAILURE CRITERION

3.1 Introduction

The general failure characteristics of a rock can be reasonably well represented by the commonly known Mohr's envelope. Therefore in the present study the Mohr's envelope is used as the basic failure criterion for the rock being cut.

The Mohr's envelope is usually constructed from experimental data. Figures 30 & 31 in Appendix IV give typical envelopes from experimental data. The shape of the envelope is different for different rocks. The exponetial form of approximation to the envelope has been used in this study. The general form of the envelope equation is

$$\tau = \tau_{\infty} - b\, e^{-\psi \sigma} \qquad (3\text{-}1)$$

3.2 Effect of Cutter Velocity

J.A. Salzer and J.F. Melaugh [1] have demonstrated in their experiments with stratapax drill blanks that the cutter velocity has an effect on the cutting force. Theoretically the effect of cutter velocity has not been clearly understood.

In the present study an attempt has been made to account for the velocity effect in calculating the shear stresses on the 'shear plane' and on the rake face. The effect has been taken to be a function of the velocity discontinuity in the case of the shear stress on the 'shear plane'. The expression assumed for the shear stress is

$$\tau_n - F_1(V^*) \qquad (3\text{-}2)$$

In the case of the shear stress on the rake face the effect is taken to be a function of the chip velocity. The assumed expression for the velocity effect is

$$\tau_t - F_2(V_c) \qquad (3\text{-}3)$$

3.3 Effect of Pore Pressure

The effect of pore pressure on the stresses on the rake face has been dealt with in Section 2.2. The pore pressure affects the stresses on the 'shear plane' also 5 . The effective normal stress on the 'shear plane' is given by the expression

$$\sigma_n - \sigma_p \qquad (3\text{-}4)$$

This is the value of the normal stress used in the construction of the Mohr's envelope.

4.0 GENERAL PLASTICITY THEORY

4.1 Conditions and Assumptions

The basic theory used in this work is the analysis of the behaviour of a continuum during plastic flow. The yield strength of the continuum varies and depends on the hydrostatic part of the stress tensor. The rock material is assumed to be rigid-plastic and isotropic. The assumption that the material is rigid-plastic implies that the elastic strain is negligible.

The flow is assumed to be a plane strain two-dimensional flow. For the (x, y, z) set of co-ordinates the strains in the z direction are considered to be negligible.

To formulate the relevant equations for plastic flow two requirements are to be met by the continuum.

a) The continuum as a whole is in dynamic equilibrium

b) The stresses at every point in the flow field obey the Tresca-Von Mises criterion of failure.

4.2 Stress Field Theory

As the stresses are predominantly compressive in the flow field, compressive stresses are considered positive and the stress element is shown in Figure 9. Using this convention the equilibrium equations are formulated as given below.

$$\frac{\partial \sigma_x}{\partial x} + \frac{\partial \tau_{xy}}{\partial y} - X = 0 \qquad (4\text{-}1)$$

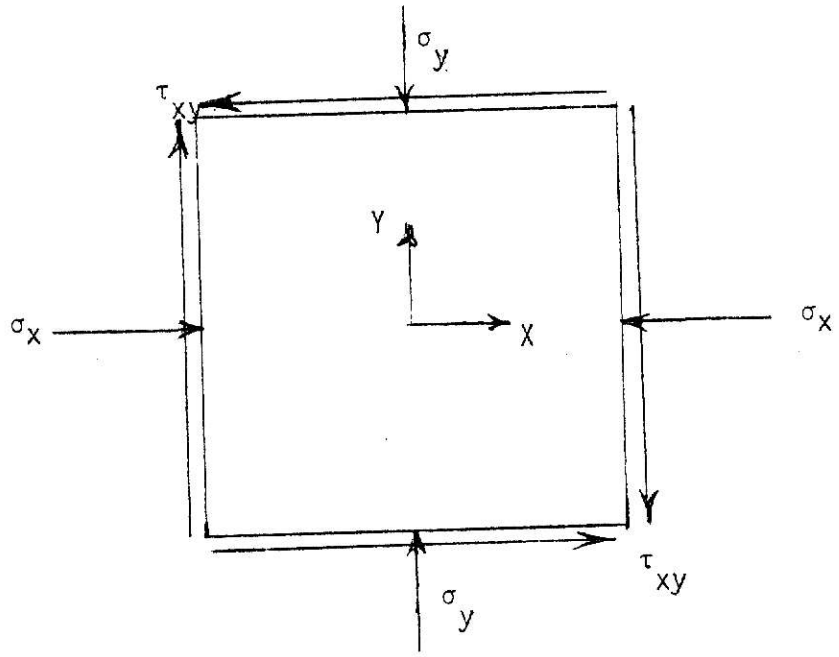

FIGURE 9 : STRESS ELEMENT

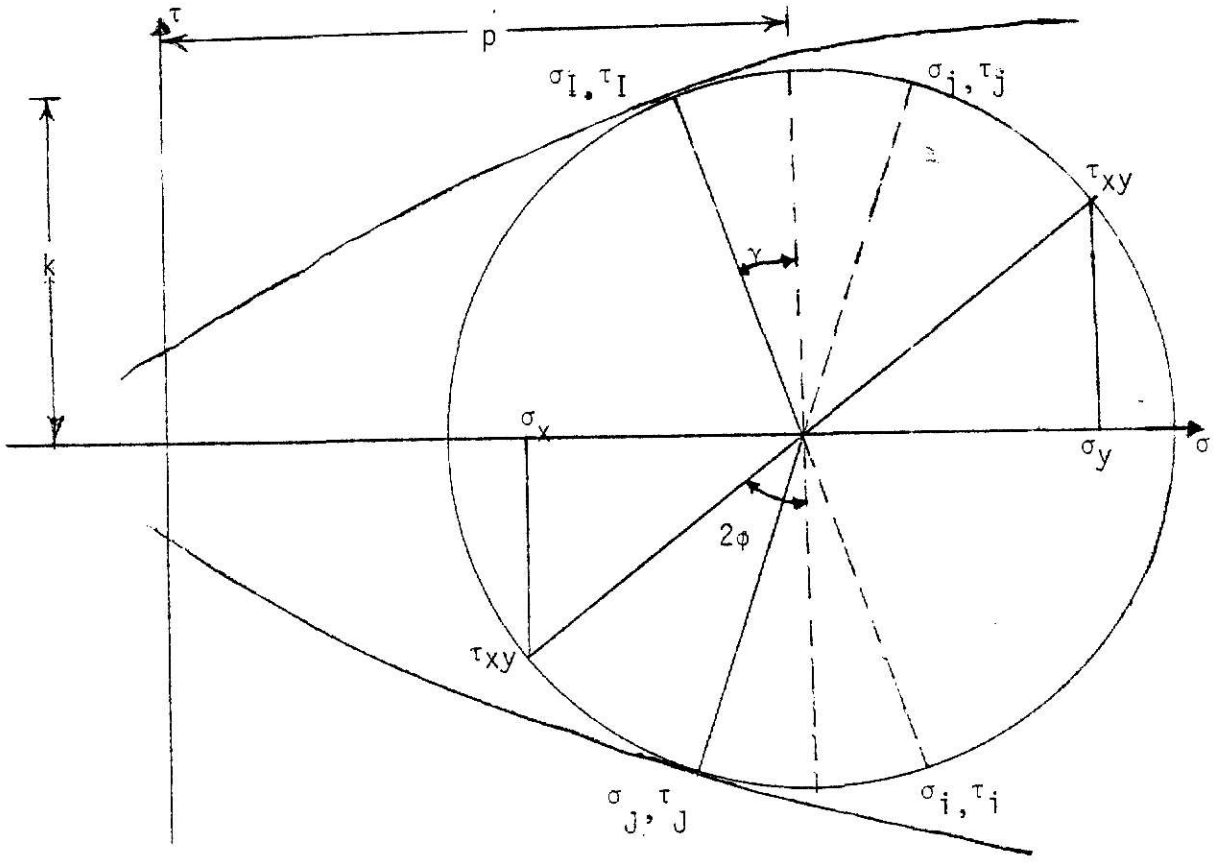

FIGURE 10 : MOHR'S CIRCLE AND MOHR'S ENVELOPE

$$\frac{\partial \sigma_y}{\partial y} + \frac{\partial \tau_{xy}}{\partial x} - Y = 0 \qquad (4\text{-}2)$$

The Tresca-Von Mises criterion of failure for the (x, y) system of co-ordinates is

$$\tau_{xy}^2 + \left[\frac{\sigma_x - \sigma_y}{2}\right]^2 = k^2 \qquad (4\text{-}3)$$

The yield shear stress k is assumed to be a known function of the hydrostatic pressure p of the stress tensor. This follows from the fact that at yield the Mohr's envelope is tangent to the Mohr's circle.

The yield criterion is satisfied by defining the stress components in the x-y plane as follows:

$$\sigma_x = p - k \sin(2\phi) \qquad (4\text{-}4)$$

$$\sigma_y = p + k \sin(2\phi) \qquad (4\text{-}5)$$

$$\tau_{xy} = k \cos(2\phi) \qquad (4\text{-}6)$$

Figure 10 shows these stress components on the Mohr's circle. The angle ϕ is measured positive in the counter clockwise direction. The angle made by the maximum normal compressive stress with the positive direction of the x axis is $(\phi + \pi/4)$. The hydrostatic pressure p is given by

$$p = \frac{\sigma_x + \sigma_y}{2} \qquad (4\text{-}7)$$

For the plane strain condition of flow the normal stress in the z direction is equal to the hydrostatic pressure p, and τ_{xz} and τ_{yz} are zero.

Differentiating (4-4), (4-5) & (4-6) according to the differentials in (4-1) & (4-2) and substituting yields the following two equations.

$$\left[1 + \sin(2\phi)\,\frac{\partial k}{\partial p}\right]\frac{\partial p}{\partial x} + \left[\cos(2\phi)\,\frac{\partial k}{\partial p}\right]\frac{\partial p}{\partial y} + 2k\cos(2\phi)\,\frac{\partial \phi}{\partial x} - 2k\sin(2\phi)\,\frac{\partial \phi}{\partial y} = X \qquad (4\text{-}8)$$

$$\left[\cos(2\phi)\,\frac{\partial k}{\partial p}\right]\frac{\partial p}{\partial x} + \left[1 + \sin(2\phi)\,\frac{\partial k}{\partial p}\right]\frac{\partial p}{\partial y} - 2k\sin(2\phi)\,\frac{\partial \phi}{\partial x} + 2k\cos(2\phi)\,\frac{\partial \phi}{\partial y} = Y \qquad (4\text{-}9)$$

These two quasilinear hyperbolic partial differential equations can be solved by the method of characteristics. This method defines two families of stress characteristics. The lines are designated by the letters i & j and along these lines the values of p and ϕ are known. The stresses at every point in the flow field are defined by these lines.

The direction derivatives are given by

$$\frac{\partial p}{\partial x}\,dx + \frac{\partial p}{\partial y}\,dy = dp \qquad (4\text{-}10)$$

$$\frac{\partial \phi}{\partial x}\,dx + \frac{\partial \phi}{\partial y}\,dy = d\phi \qquad (4\text{-}11)$$

Solving (4-8), (4-9), (4-10) & (4-11) by the method of

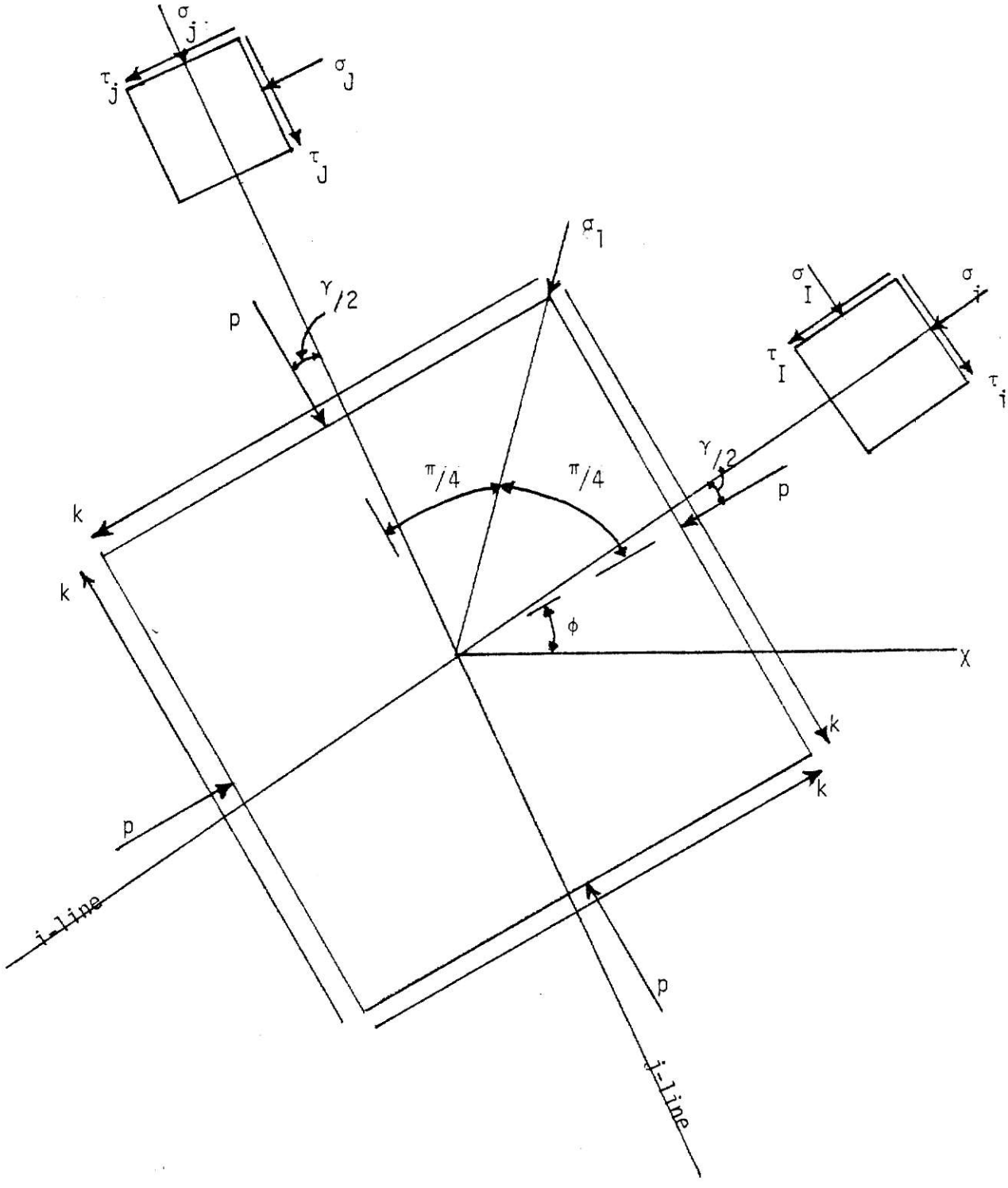

FIGURE 11: ORIENTATION OF STRESS CHARACTERISTICS ON THE BASIC STRESS ELEMENT.

characteristics, the slopes of the i and j lines are found to be

$$\frac{dy}{dx} = \tan(\phi + \gamma/2) \tag{4-12}$$

$$\frac{dy}{dx} = \tan(\phi - \gamma/2 + \pi/2) \tag{4-13}$$

The value of $\gamma/2$ is defined by the expression

$$\gamma/2 = \frac{1}{2} \sin^{-1} \frac{\partial k}{\partial p} \tag{4-14}$$

Figure 11 gives the orientation of the stress characteristics with respect to the element. The stresses (σ_I, τ_I) and (σ_J, τ_J) on these characteristics are also indicated. The stress components (σ_I, τ_I) and (σ_J, τ_J) are shown in the Mohr's circle in Figure 10.

4.3 Velocity Field Theory

The plane strain two-dimensional plastic flow problem is not completely solved until the velocity field solution is satisfied in addition to the stress field solution.

The velocity field theory will be formulated separately for two different cases. The property of the continuum for the two cases are

a) The continuum is assumed to be incompressible and the principal axes of stress and strain coincide.

b) The continuum is assumed to be compressible.

In both the theories the yield shear stress k is the same known

function of the hydrostatic pressure p. However, the orientation of the velocity field is different for the two cases.

4.3.1 Incompressible Theory

For an incompressible continuum the continuity equation is given by

$$\frac{\partial u}{\partial x} + \frac{\partial v}{\partial y} = 0 \qquad (4\text{-}15)$$

When the principal axes of stress and strain coincide, for a rigid plastic material, the angle 2ϕ for the incompressible case can be written in terms of the strain rate as

$$\tan(2\phi) = \frac{\sigma_x - \sigma_y}{2\tau_{xy}} = \frac{-\left[-\frac{\partial u}{\partial x} + \frac{\partial v}{\partial y}\right]}{-\left[+\frac{\partial u}{\partial y} + \frac{\partial v}{\partial x}\right]} \qquad (4\text{-}16)$$

The relation for angle 2ϕ is illustrated in Figure 12. Rearranging (4-16) yields a partial differential equation.

$$\left[\frac{\partial v}{\partial x} + \frac{\partial u}{\partial y}\right] + \left[\frac{\partial u}{\partial x} - \frac{\partial v}{\partial y}\right]\cot(2\phi) = 0 \qquad (4\text{-}17)$$

The directional derivatives are given by the following two equations.

$$\frac{\partial v}{\partial x}\,dx + \frac{\partial v}{\partial y}\,dy = dv \qquad (4\text{-}18)$$

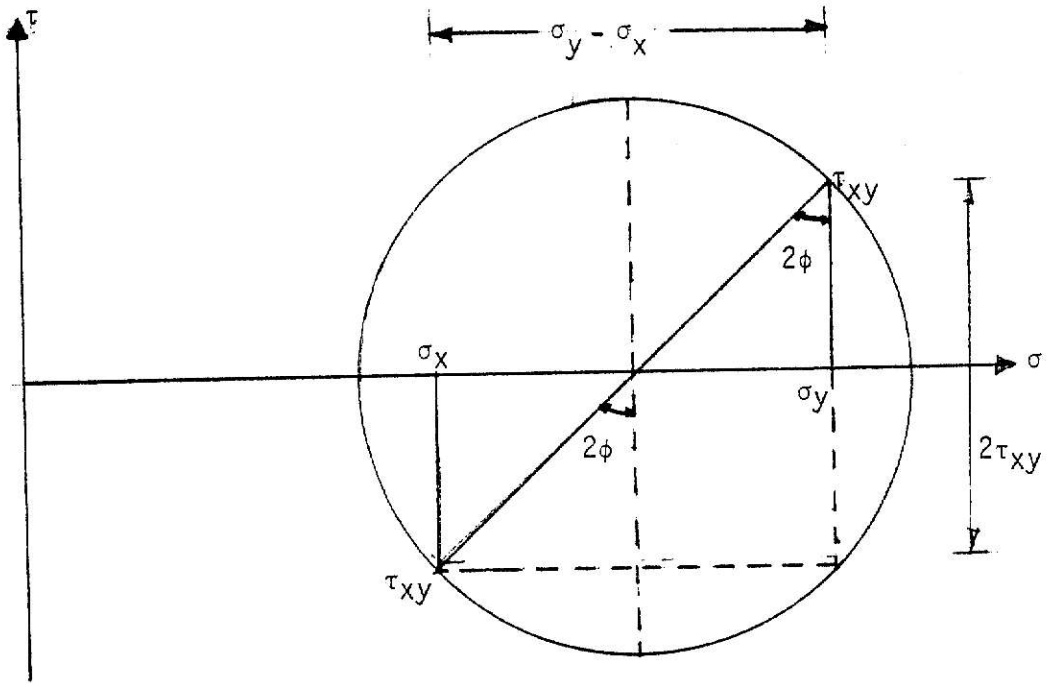

FIGURE 12a : MOHR'S CIRCLE FOR STRESS

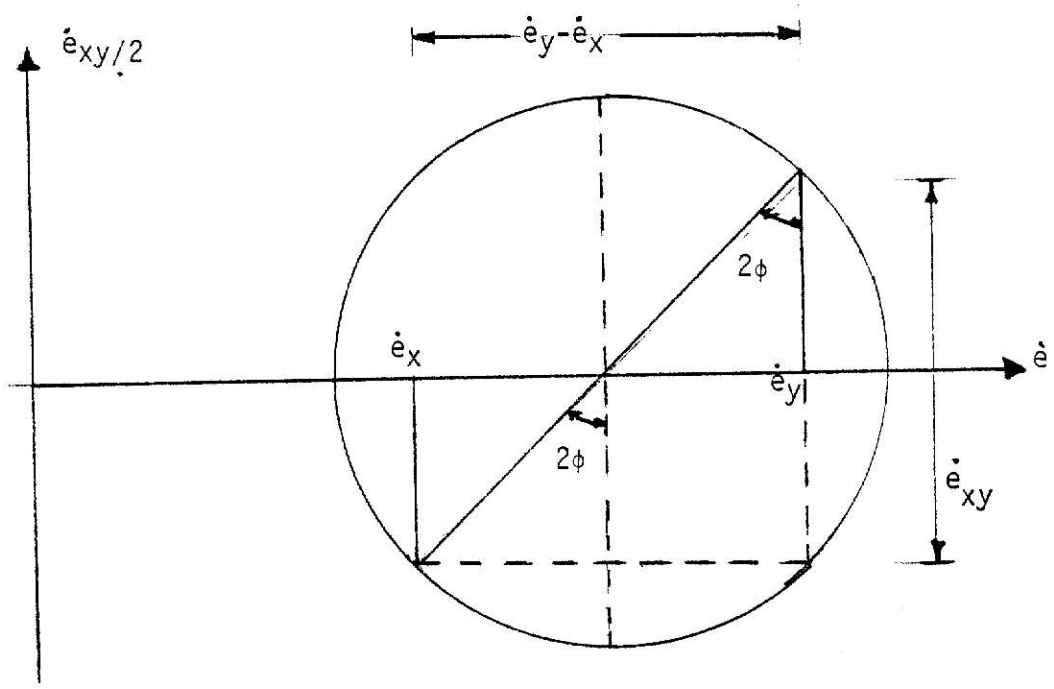

FIGURE 12b : MOHR'S CIRCLE FOR STRAIN RATE

$$\frac{\partial u}{\partial x} dx + \frac{\partial u}{\partial y} dy = du \qquad (4\text{-}19)$$

Solving (4-15), (4-17), (4-18) & (4-19) by the method of chracteristics, the slopes of the velocity characteristics are

$$\frac{\partial y}{\partial x} = \tan(\phi) \qquad (4\text{-}20)$$

$$\frac{\partial y}{\partial x} = \tan(\phi + \pi/2) \qquad (4\text{-}21)$$

The orientation of the velocity field and stress field for the incompressible theory is shown in Figure 13. The velocity characteristics do not coincide with the stress characteristics in this case. The angle between them is $\gamma/2$.

4.3.2 Compressible Theory

This method is based on the principle of plastic potential. According to this principle the stress and strain rate during plastic flow are related by the following expressions.

$$\dot{e}_x = \lambda \frac{\partial f}{\partial \sigma_x} \qquad (4\text{-}22)$$

$$\dot{e}_y = \lambda \frac{\partial f}{\partial \sigma_y} \qquad (4\text{-}23)$$

$$\dot{e}_{xy} = \lambda \frac{\partial f}{\partial \tau_{xy}} \qquad (4\text{-}24)$$

f is the yield surface criterion given by the expression

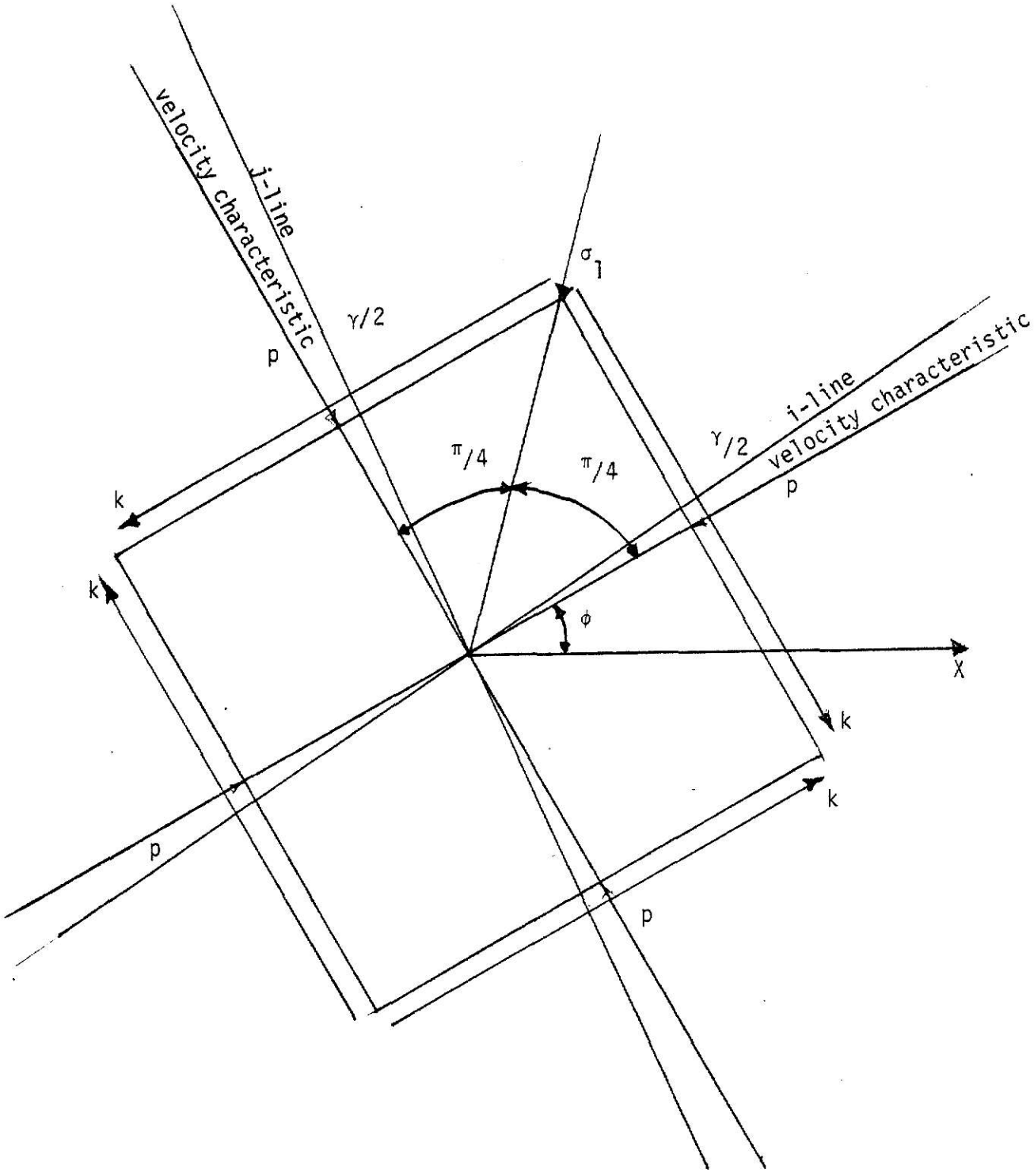

FIGURE 13 : STRESS AND VELOCITY CHARACTERISTICS FOR THE INCOMPRESSIBLE THEORY.

$$f = \tau_{xy}^2 + \left[\frac{\sigma_x - \sigma_y}{2}\right]^2 - k^2 \tag{4-25}$$

The compressive strain rates are related to the velocity by the expressions

$$\dot{e}_x = - \frac{\partial u}{\partial x} \tag{4-26}$$

$$\dot{e}_y = - \frac{\partial v}{\partial y} \tag{4-27}$$

$$\dot{e}_{xy} = - \left[\frac{\partial u}{\partial y} + \frac{\partial v}{\partial x}\right] \tag{4-28}$$

Using equations (4-22) through (4-28) and (4-2) through (4-6) the following two quasilinear hyperbolic partial differential equations are obtained.

$$\left[\frac{\partial u}{\partial x} - \frac{\partial v}{\partial y}\right] \cot(2\phi) + \frac{\partial v}{\partial x} + \frac{\partial u}{\partial y} = 0 \tag{4-29}$$

$$\left[\frac{\partial v}{\partial x} + \frac{\partial u}{\partial y}\right] \sec(2\phi) \frac{\partial k}{\partial p} + \frac{\partial u}{\partial x} + \frac{\partial v}{\partial y} = 0 \tag{4-30}$$

Solving (4-29), (4-30), (4-18) & (4-19) by the method of characteristics, the slopes of the velocity characteristics are

$$\frac{dy}{dx} = \tan(\phi + \gamma/2) \tag{4-31}$$

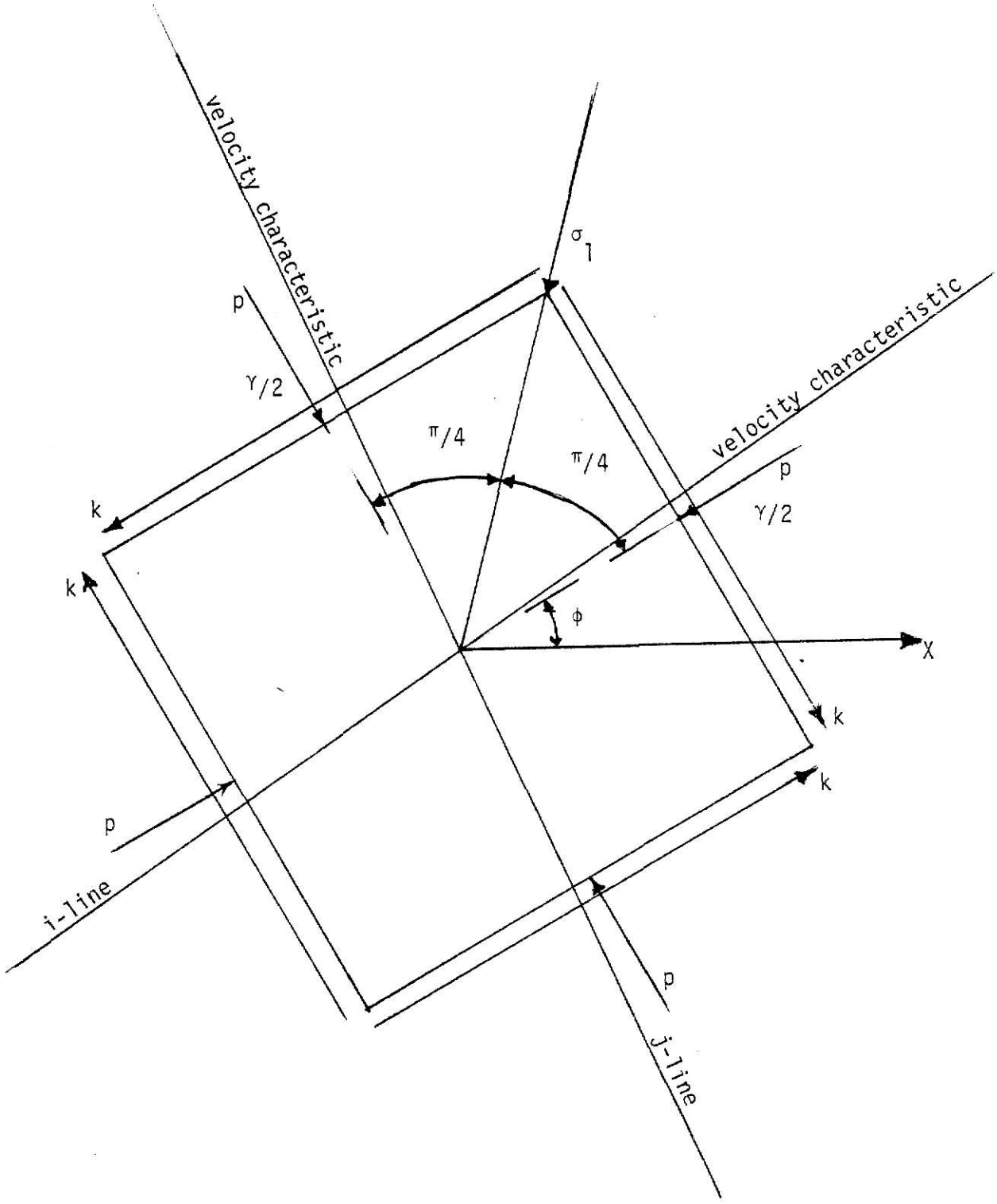

FIGURE 14 : STRESS AND VELOCITY CHARACTERISTICS FOR THE COMPRESSIBLE THEORY.

$$\frac{dy}{dx} = \tan(\phi - \gamma/2 + \pi/2) \qquad (4\text{-}32)$$

Figure 14 shows the orientation of the velocity characteristics and stress characteristics with respect to the stress element. In this case the velocity and stress characteristics coincide.

The cutting problem is solved separately by the two theories formulated above to determine if there is any significant difference in the predicted cutting forces.

5.0 INCOMPRESSIBLE THEORY SOLUTION

5.1 Failure Criterion

The theory introduced in the previous chapter is now applied to the yielding which occurs along the 'shear plane' in the cutting problem. The 'shear plane' is a velocity characteristic. The velocity discontinuity occurs along this line but its direction is not necessarily parallel to the velocity characteristic. Figure 15 gives the basic stress element corresponding to the incompressible case on the 'shear plane' and Figure 16 gives the corresponding Mohr's circle. For this case the stress and velocity characteristics do not coincide. The normal and shear stresses on the 'shear plane' are the stresses corresponding to the maximum point on the Mohr's circle. The stresses on the i line rotated by an angle of $\gamma/2$ in the clockwise direction gives the stresses on the 'shear plane'. This is indicated in Figures 15 & 16.

Based on the velocity effect and pore pressure effect discussed in Chapter 3.0 the normal and shear stress on the Mohr's circle are given by

$$\sigma_n - \sigma_{pl} = \sigma + \tan(\gamma)\ \tau \qquad (5\text{-}1)$$

$$\tau_n - F_1(V^*) = \frac{\tau}{\cos(\gamma)} \qquad (5\text{-}2)$$

The equation to the envelope is

$$\tau = \tau_\infty - b\, e^{-\psi \sigma} \qquad (5\text{-}3)$$

The values of τ and σ are obtained by simultaneously solving (5-1), (5-2) & (5-3). Differentiating equation (5-3) with respect to angle γ yields

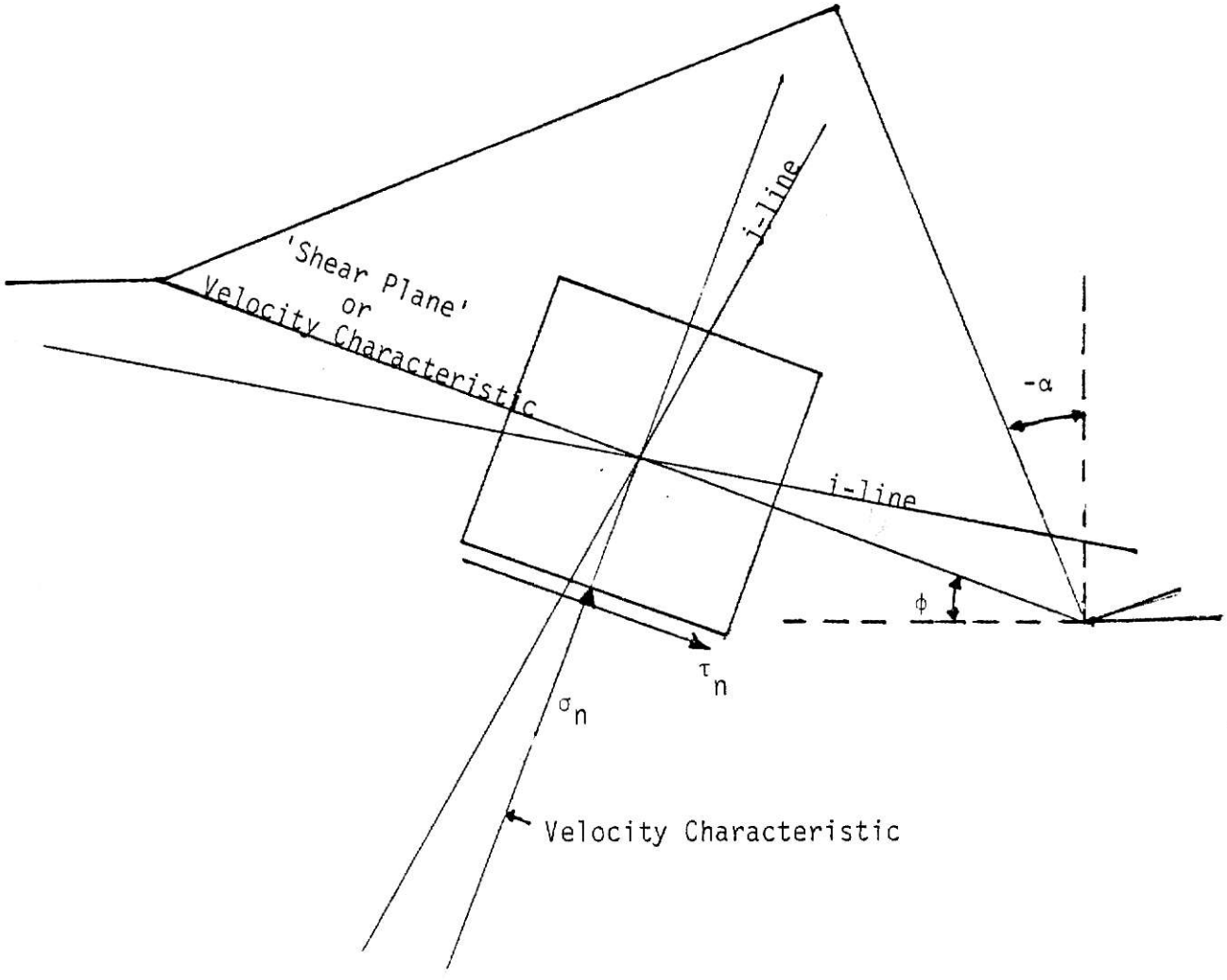

FIGURE 15 : STRESS ELEMENT FOR THE INCOMPRESSIBLE SOLUTION

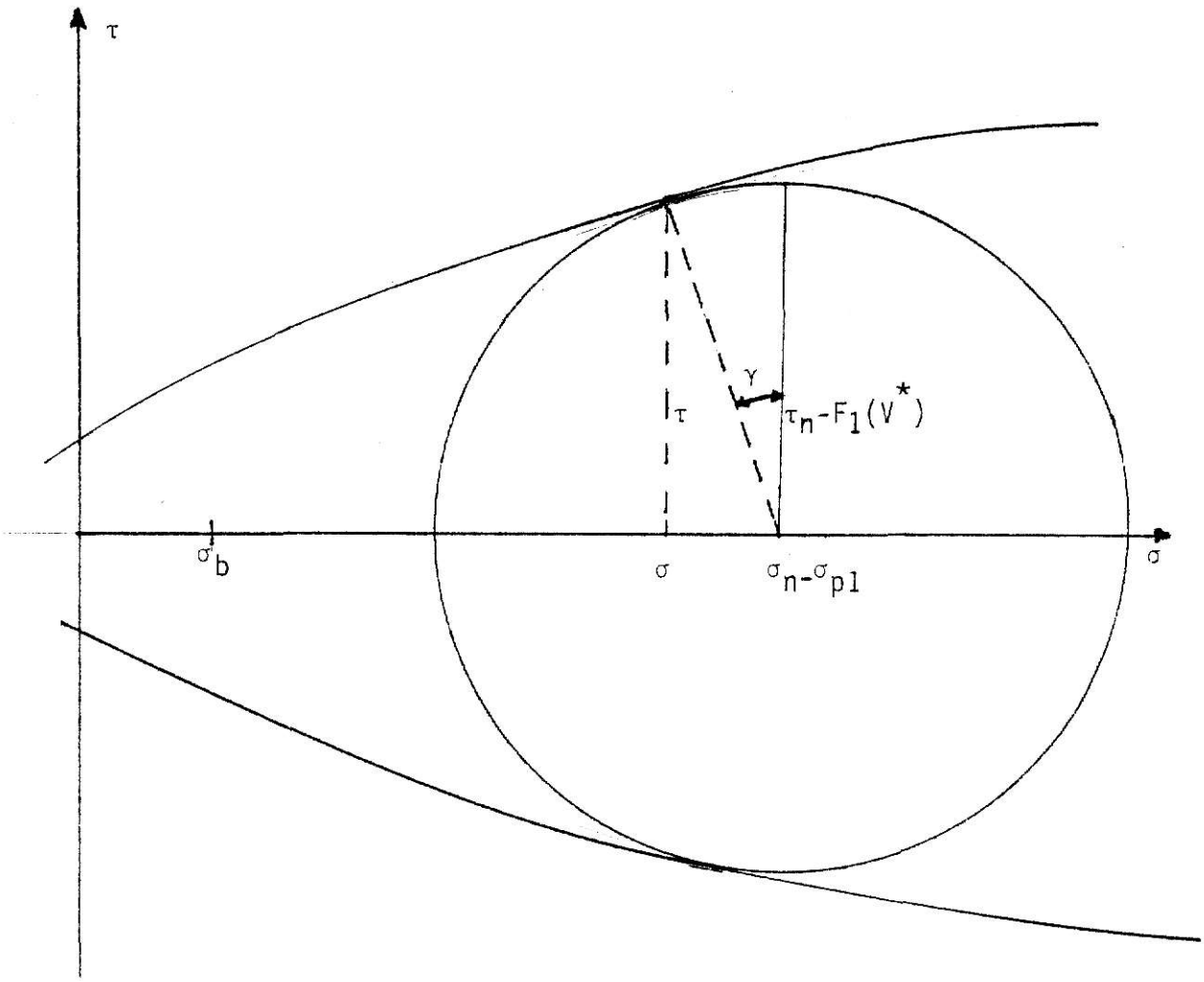

FIGURE 16 : MOHR'S CIRCLE FOR INCOMPRESSIBLE SOLUTION

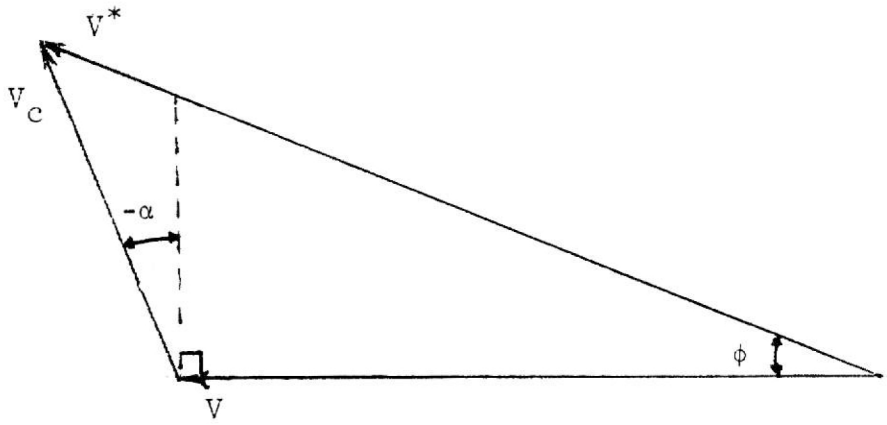

FIGURE 17 : HODOGRAPH FOR THE INCOMPRESSIBLE THEORY

$$\frac{d\tau}{d\gamma} = b\ \psi\ e^{-\psi\sigma} = \tan(\gamma) \qquad (5\text{-}4)$$

A particular value of σ is assumed and the following parameters are calcualted from the relevant expressions.

(i) Angle γ from (5-4)

(ii) τ from (5-3)

(iii) τ_n from (5-2)

(iv) σ_n from (5-1)

5.2 Velocity Relation and Hodograph

For the incompressible case the other velocity characteristic is perpendicular to the 'shear plane'. Hence the condition that the velocity discontinuity has its direction perpendicular to the other characteristic makes its direction along the 'shear plane'. The hodograph is shown in Figure 17. The velocity of the chip and the velocity discontinuity are given by the expressions

$$V_c = \frac{\sin(\phi)}{\cos(\phi - \alpha)}\ V \qquad (5\text{-}5)$$

$$V^* = \frac{\cos(\alpha)}{\cos(\phi - \alpha)}\ V \qquad (5\text{-}6)$$

5.3 Method of Solution

A numerical procedure is adopted to find the cutting forces on the tool corresponding to the state of minimum energy. The procedure consists of three iterations; one to find the values of σ_n and τ_n to fit the Mohr's

envelope; the second to find the values of θ at which equilibrium conditions and failure criterion are satisfied simultaneously; the third to find the value of ϕ at which the force per unit area F_t/t is minimum.

The Mohr's envelope is constructed from experimental data and for the approximate envelope the values of τ_∞, b & ψ in equation (5-3) are determined by curve fitting.

A value for the rake angle α is chosen and a particular value for ϕ and θ are picked. The stresses on the tool σ_t and τ_t are calculated from (2-5) and (2-9).

The normal and shear stress on the 'shear plane' must have values which simultaneously satisfy equilibrium conditions and failure criterion. In order to differentiate the stresses formulated from equilibrium conditions and failure criterion they are denoted as follows:

σ_n^* & τ_n^* - from equilibrium conditions.

σ_n & τ_n - from failure criterion.

The values of σ_n is calculated from equation (2-7). To satisfy the failure criterion an error function is defined as

$$\varepsilon(\sigma) = \sigma_n^* - \sigma_n \qquad (5\text{-}7)$$

A Newton iteration is performed on the value of σ to make the error function $\varepsilon(\sigma)$ small.

The value of τ_n is calculated from (2-6) and an iteration is performed on the value of θ to make the error function $\varepsilon(\theta)$, defined by the expression $(\tau_n^* - \tau_n)$, very small.

An iteration is performed on the value of ϕ to obtain the minimum

value of F_t/t. For each value of ϕ, the iterations on σ and θ are performed, which is a necessacity to satisfy the equilibrium conditions and failure criterion.

The computer program in Appendix I performs the numerical procedure outlined in this chapter.

6.0 COMPRESSIBLE THEORY SOLUTION

6.1 Failure Criterion

Figure 18 shows the basic compressible theory stress element on the 'shear plane'. The element is at an angle γ in the clockwise direction from the 'shear plane'. In this case the velocity and stress characteristics coincide. The Mohr's circle is shown in Figure 19. The normal and shear stresses on the 'shear plane' are the stresses corresponding to the point at which the Mohr's envelope is tangent to the Mohr's circle. The normal and shear stresses in the Mohr's circle are given by

$$\sigma_n - \sigma_{pl} = \sigma \tag{6-1}$$

$$\tau_n - F_1(V^*) = \tau \tag{6-2}$$

The equation to the envelope is given by

$$\tau = \tau_\infty - be^{-\psi\sigma} \tag{6-3}$$

The values of σ and τ are found by simultaneously solving (6-1), (6-2) & (6-3).

6.2 Velocity Relations and Hodograph

The velocity discontinuity for the compressible case does not occur in the direction of the 'shear plane'. The orientation of V^* is in a direction perpendicular to the other velocity characteristic. The hodograph is shown in Figure 20. The velocity of the chip and the velocity discontinuity are given by the following expressions.

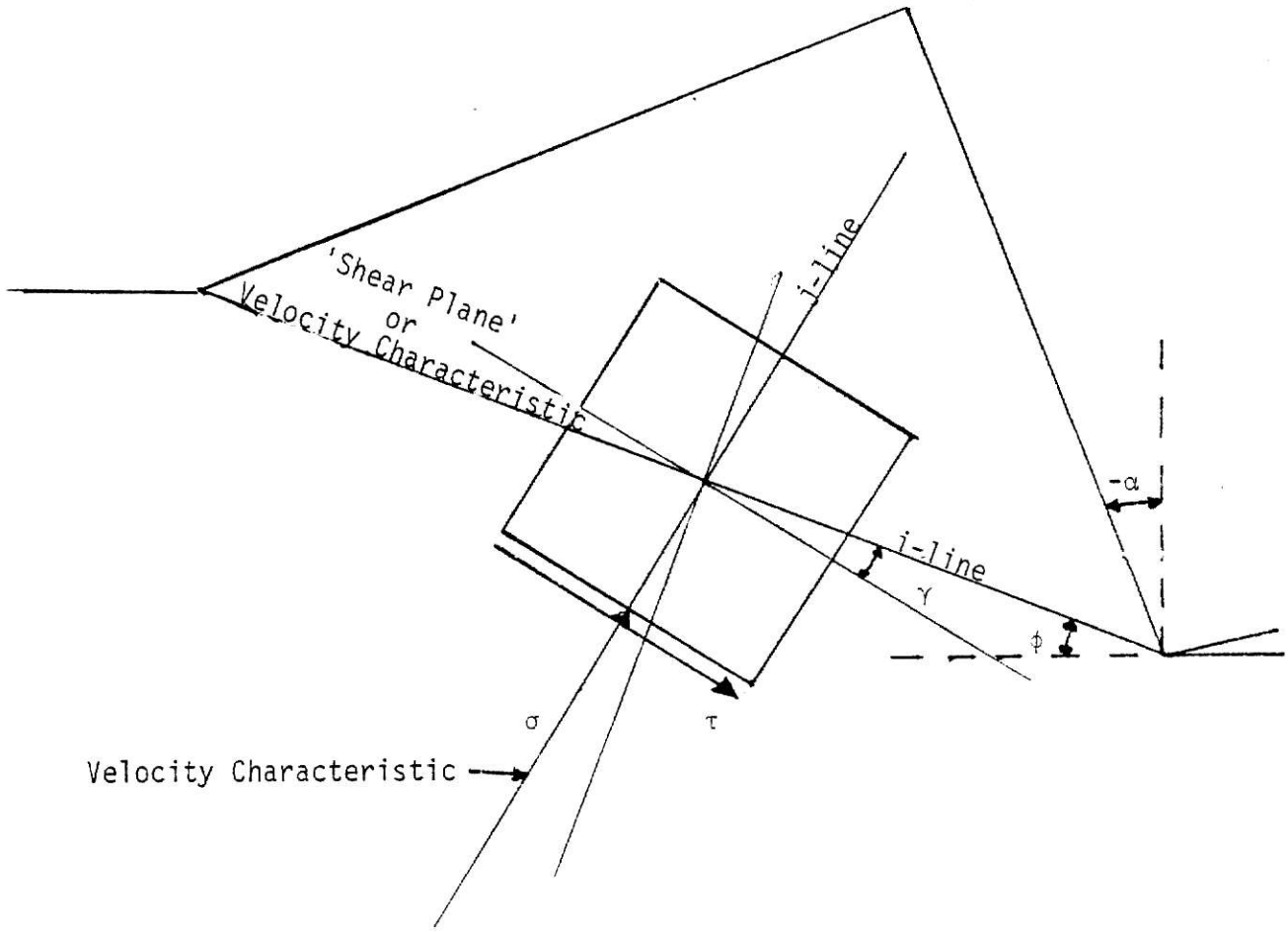

FIGURE 18 : STRESS ELEMENT FOR COMPRESSIBLE SOLUTION

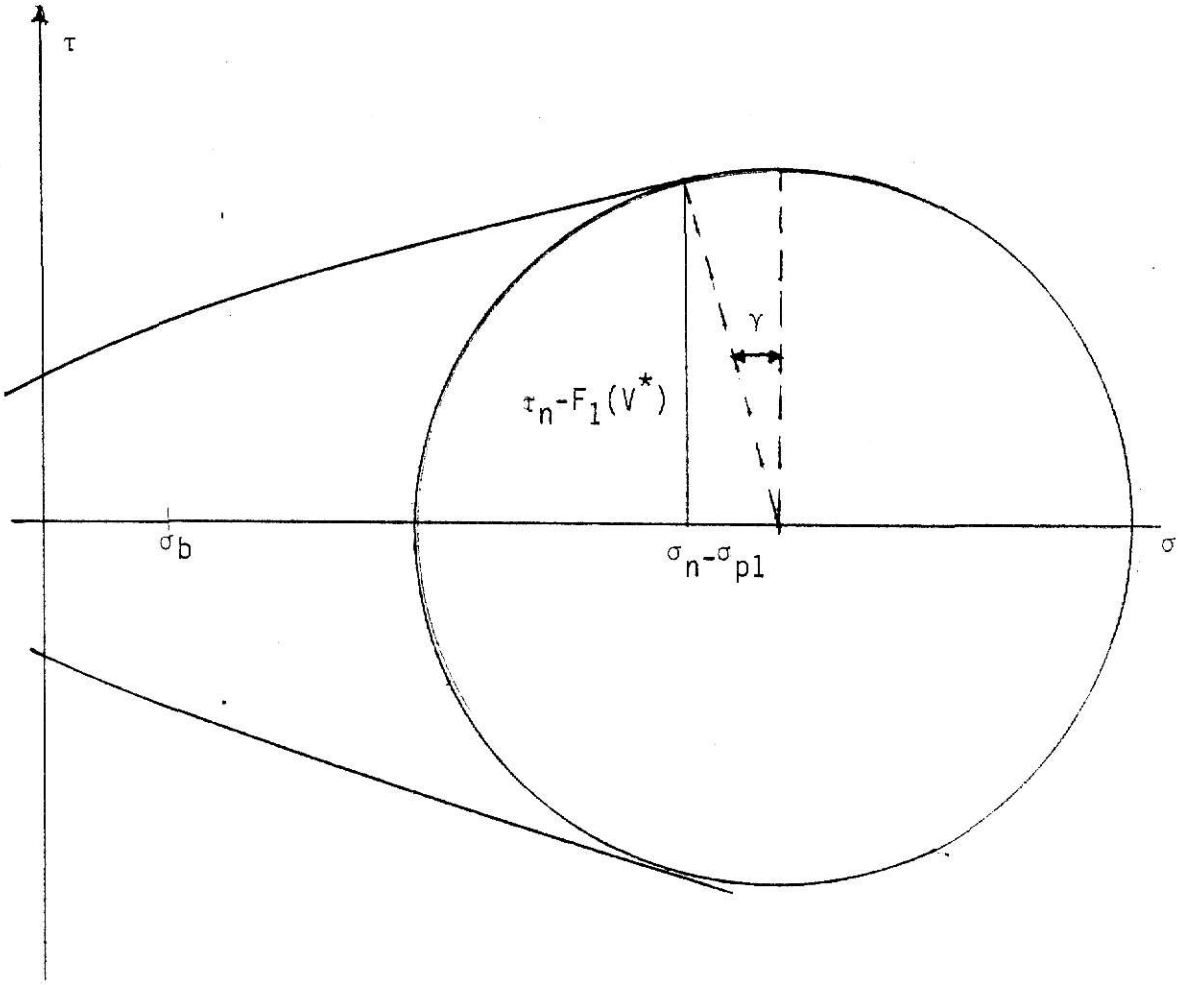

FIGURE 19 : MOHR'S CIRCLE FOR COMPRESSIBLE SOLUTION

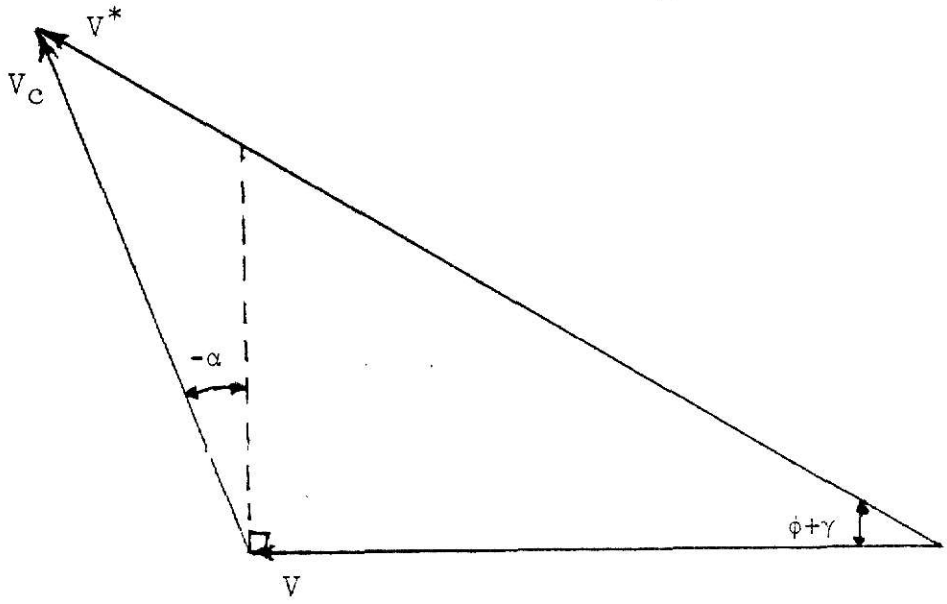

FIGURE 20 : HODOGRAPH FOR THE COMPRESSIBLE THEORY

$$V_c = \frac{\sin(\phi + \gamma)}{\cos(\phi - \alpha + \gamma)} \quad V \qquad (6\text{-}4)$$

$$V^* = \frac{\cos(\alpha)}{\cos(\phi - \alpha + \gamma)} \quad V \qquad (6\text{-}5)$$

5.3 Method of Solution

The numerical procedure is similar to that for the incompressible solution. The only difference is that the values of the stresses on the 'shear plane' are those corresponding to the tangential point and hence there is no iteration involved to calculate the values of σ_n and τ_n to fit the Mohr's envelope. The rest of the procedure is the same to find the values of θ and ϕ for minimum cutting energy.

The computer program in Appendix II performs the numerical procedure outlined in this chapter.

7.0 COMPARISON WITH EXPERIMENTAL RESULTS

7.1 Introduction

The validity of the cutting theory as a tool to improve the design of PDC bits is best analysed by comparing the predicted results with experimental data from studies on the performance of PDC cutters to cut shale. The work done by J.B. Cheatham and W.H. Daniel [2] and the work by J.F. Melaugh and J.A. Salzer [1] are compared in this study. The incompressible theory solution is used to predict the cutting forces.

The effect of friction is not incorporated in the theory. The value of μ is found by trial and error. The factor which controls the value of μ is the necessary condition for all shear stresses to be within the Mohr's envelope.

7.2 Comparison with Cheatham's Experimental Results

J.B. Cheatham 2 conducted experiments on single cutters to cut shale. The velocity of the cutter was small (2 cm/ sec) and hence it is assumed that the velocity effect on the cutting force in the present comparitive study is negligible.

For comparision the parameters such as confining pressure, area of cut and rake angle were given the same values in the theory as Cheatham had in his experiments. The rock material used in the study was Mancos Shale and the Mohr's envelope was drawn from Cheatham's experimental tests.

Table 1 shows the theoretical results from the incompressible theory solution for a 0.38" rectangular tool with a depth of cut of 0.01".

TABLE 1 : THEORETICAL RESULTS FOR THE INCOMPRESSIBLE SOLUTION
VELOCITY EFFECT IS ZERO.

FRICTION COEFFICIENT μ	0.4	0.3	0.2	0.1
NORMAL STRESS ON THE SHEAR PLANE σ_n psi	7820.38	5794.90	4966.80	4225.30
SHEAR STRESS ON THE SHEAR PLANE τ_n psi	6707.66	5148.79	4507.90	3915.70
NORMAL STRESS ON THE TOOL FACE σ_t psi	13109.49	11551.90	11335.38	11075.90
SHEAR STRESS ON THE TOOL FACE τ_t psi	5243.79	3465.60	2267.07	1107.60
TANGENTIAL FORCE PER UNIT AREA F_t/t	30025.31	21512.48	15747.95	11747.40
NORMAL FORCE PER UNIT AREA F_n/t	14211.41	7896.20	3836.93	1438.50
ANGLE ϕ degrees	15.47	16.18	19.38	22.29
ANGLE θ degrees	40.79	36.17	19.38	22.29

The confining pressure is 2030 psi and the pore pressure is considered negligible. The rake angle is 0 degrees.

Cheatham's experimental results show that for a cutter depth of 0.01" the range of F_t/t is approximately 13040 psi to 19405 psi. In the present study the value of F_t/t depends on the friction factor μ. For the cutter depth of 0.01" and for a range of μ from 0.1 to 0.3 the range of F_t/t is 11750 psi to 21513 psi. In F_t/t there is good agreement between the theoretical results and Cheatham's experimental results.

7.3 Comparison with Melaugh's Experimental Results

J.F. Melaugh [1] conducted experiments with stratapax blanks to cut Mancos shale. The velocity of the cutter was much higher (140 fpm and 350 fpm) than that in Cheatham's experiments. The cutting forces in Melaugh's experiments are much higher than those in Cheatham's experiments. This appears to be partially due to the velocity effect.

The Mohr's envelope was constructed from experimental results of Melaugh. The cutter area is 0.004 in^2 and the confining pressure is 10000 psi. Figure 21 shows the comparision of rake angle vs cutting force for a cutter velocity of 140 fpm. The numerical results are shown in Table 2 in Appendix III. Figure 22 shows the same graph for a cutter velocity of 350 fpm and Table 3 in Appendix III gives the corresponding numerical results. Figure 23 shows the variation of friction factor μ in relation to the rake angle α for two velocities. The value of μ has been found by trial and error to satisfy the Mohr's envelope.

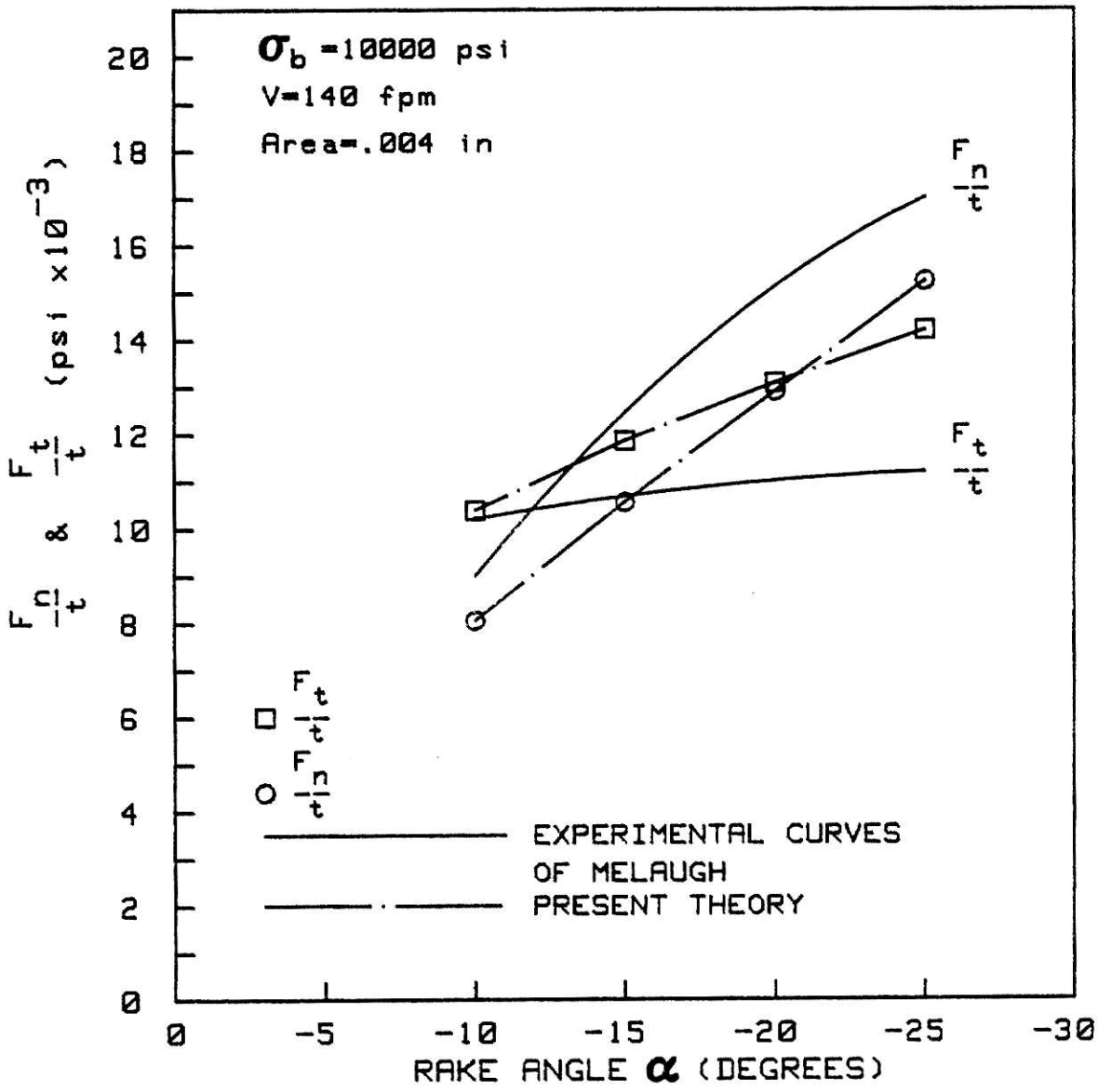

FIGURE 21 : THEORETICAL CUTTING FORCES IN COMPARISION WITH MELAUGH'S RESULTS FOR V = 140 fpm.

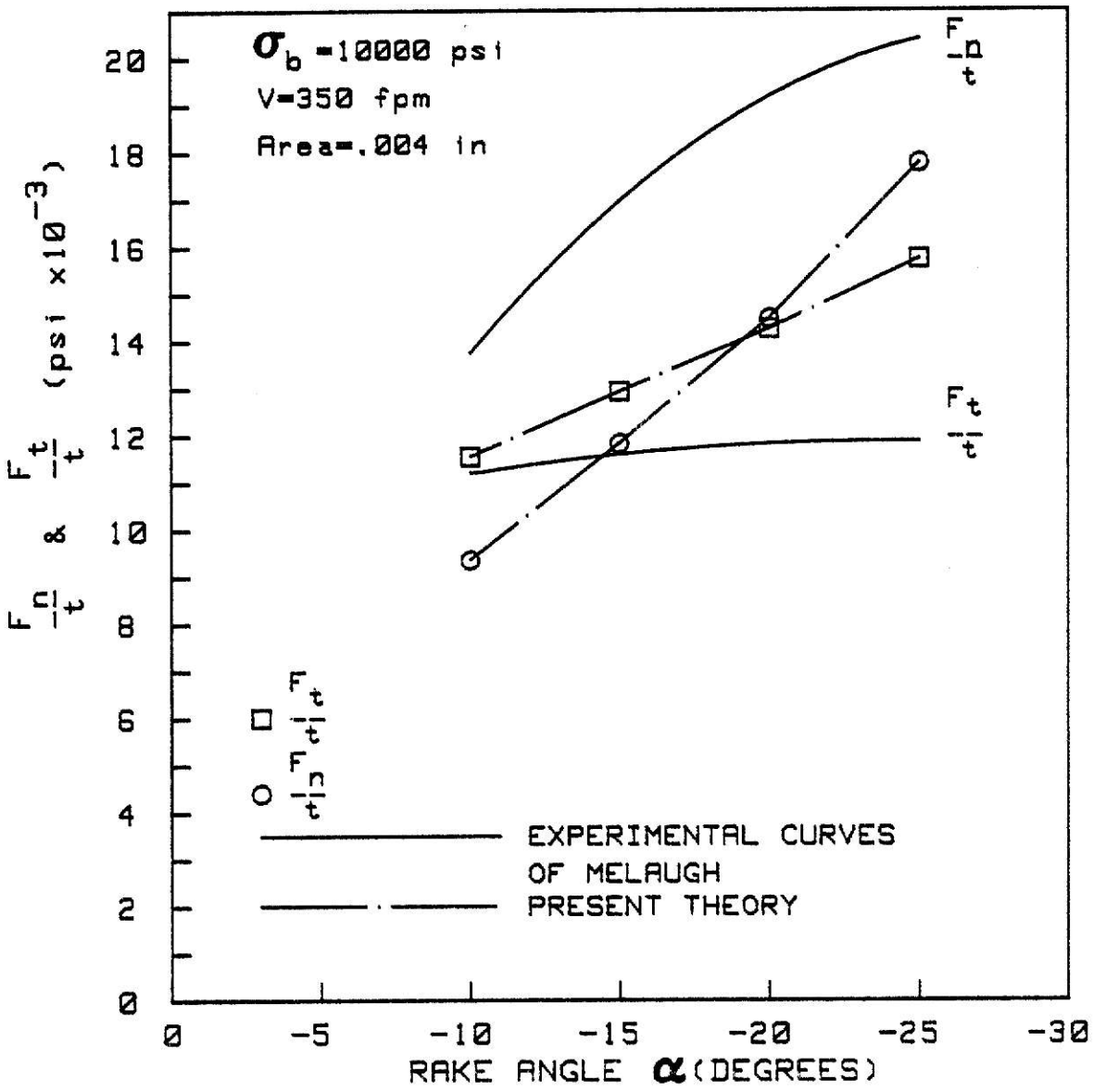

FIGURE 22 : THEORETICAL CUTTING FORCES IN COMPARISION WITH MELAUGH'S RESULTS FOR V = 350 fpm.

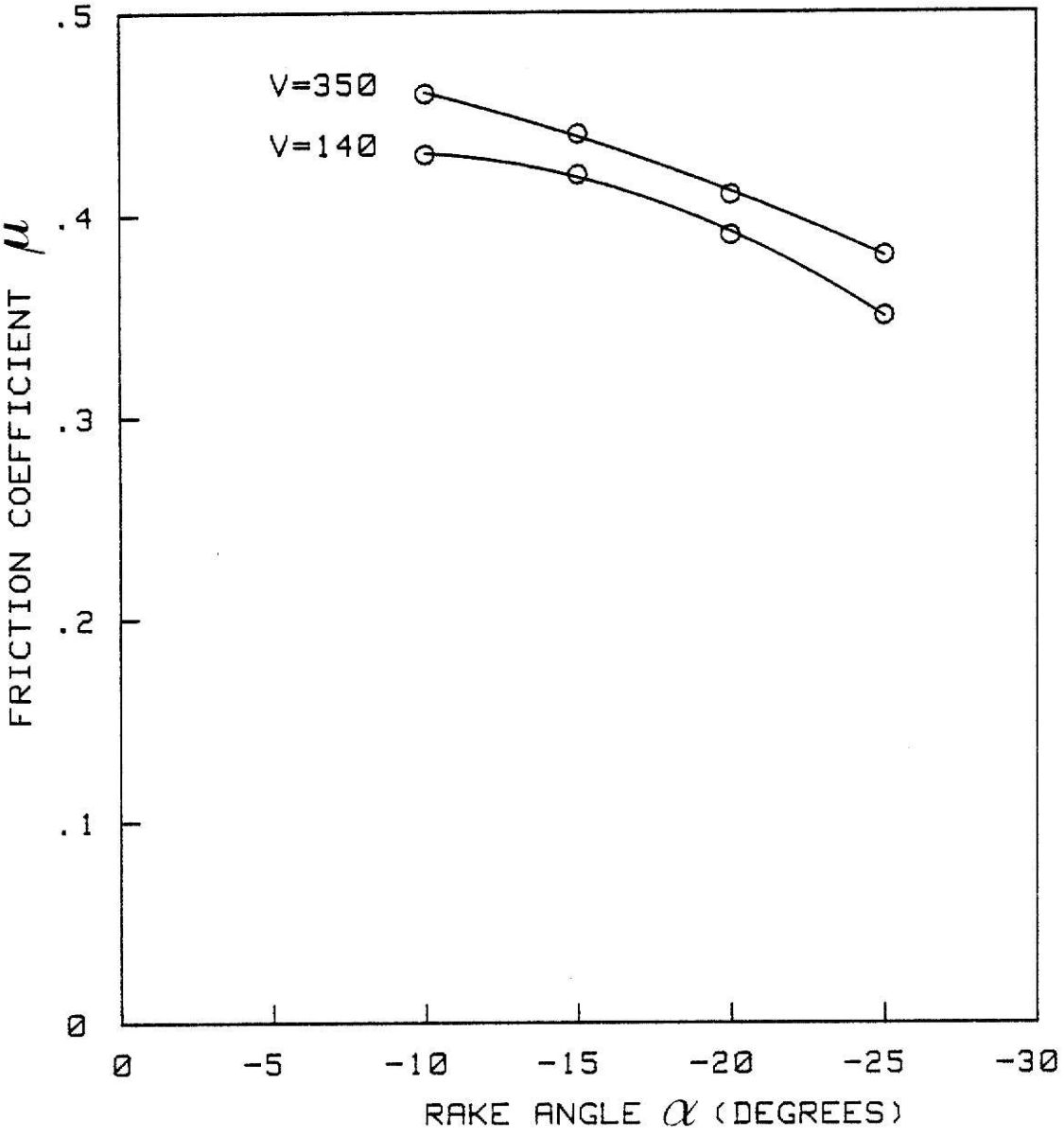

FIGURE 23 : RAKE ANGLE vs FRICTION COEFFICIENT FOR TWO DIFFERENT VELOCITIES.

8.0 COMPARISON BETWEEN THE TWO THEORIES

A comparitive study of the results obtained by the incompressible theory solution and the compressible theory solution was done for the same rock properties and confining pressure. Figure 24 shows the graph of cutting force vs rake angle for a cutter velocity of 140 fpm for the two theories. The corresponding numerical results are given in Tables 4, 5 & 6 in Appendix III. Figure 25 shows the same graph for a cutter velocity of 350 fpm and the corresponding results are shown in Tables 7, 8 & 9 in Appendix III.

For the Mancos shale rock material considered in this study the two theories show similar results and their differences are not very significant. A possible reason is that the mean stress is large and the Mohr's circle is far from the origin where the slope of the Mohr's envelope is small and hence the angle γ in the Mohr's circle is small. This makes the the maximum shear stress in the Mohr's circle close to the tangential point.

The results of the two theories may differ more for other rock materials in which the stresses are not as high or the slope of the envelope is very large.

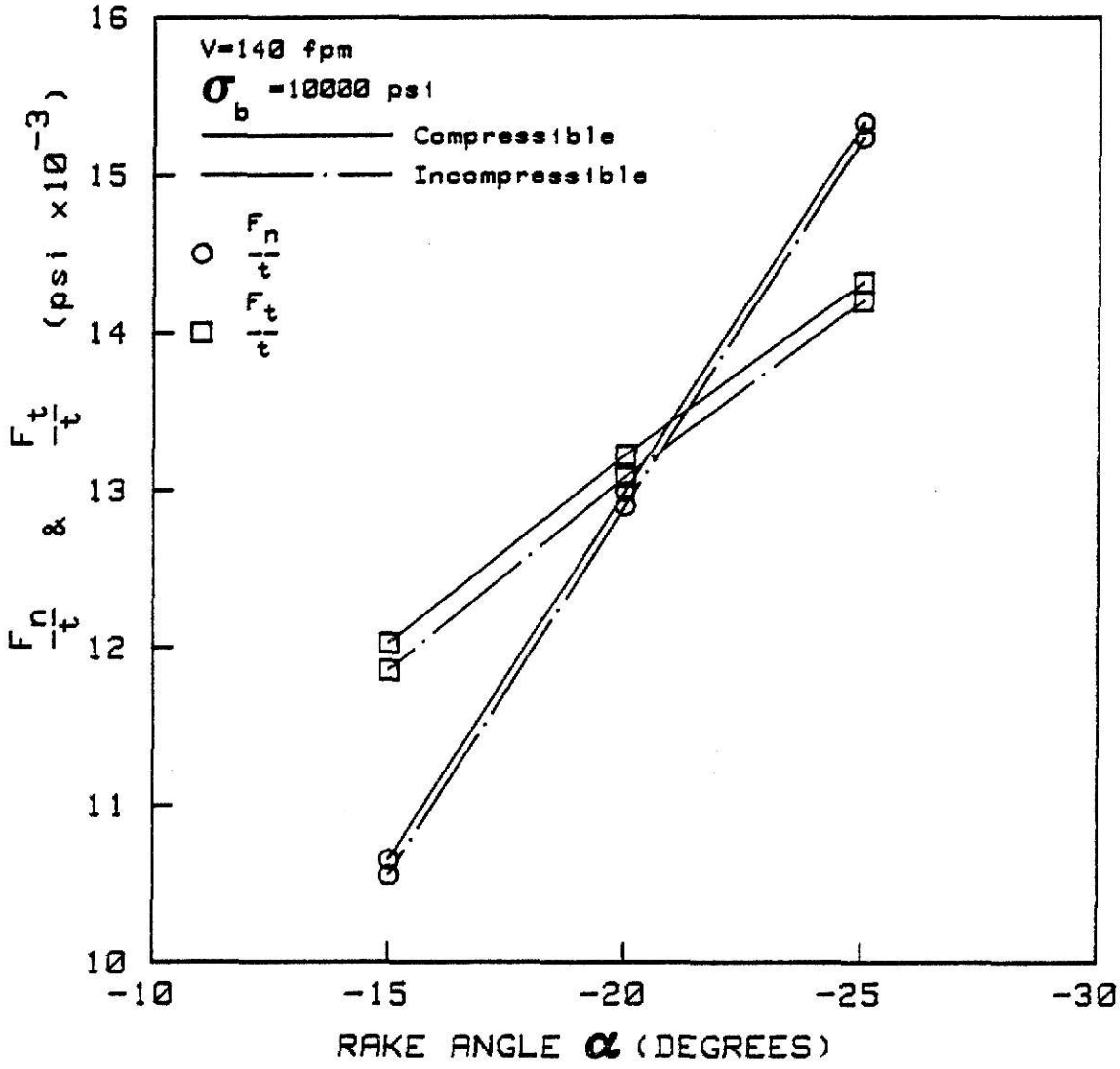

FIGURE 24 : THEORETICAL CUTTING FORCES FROM THE TWO PLASTICITY THEORIES FOR V = 140 fpm.

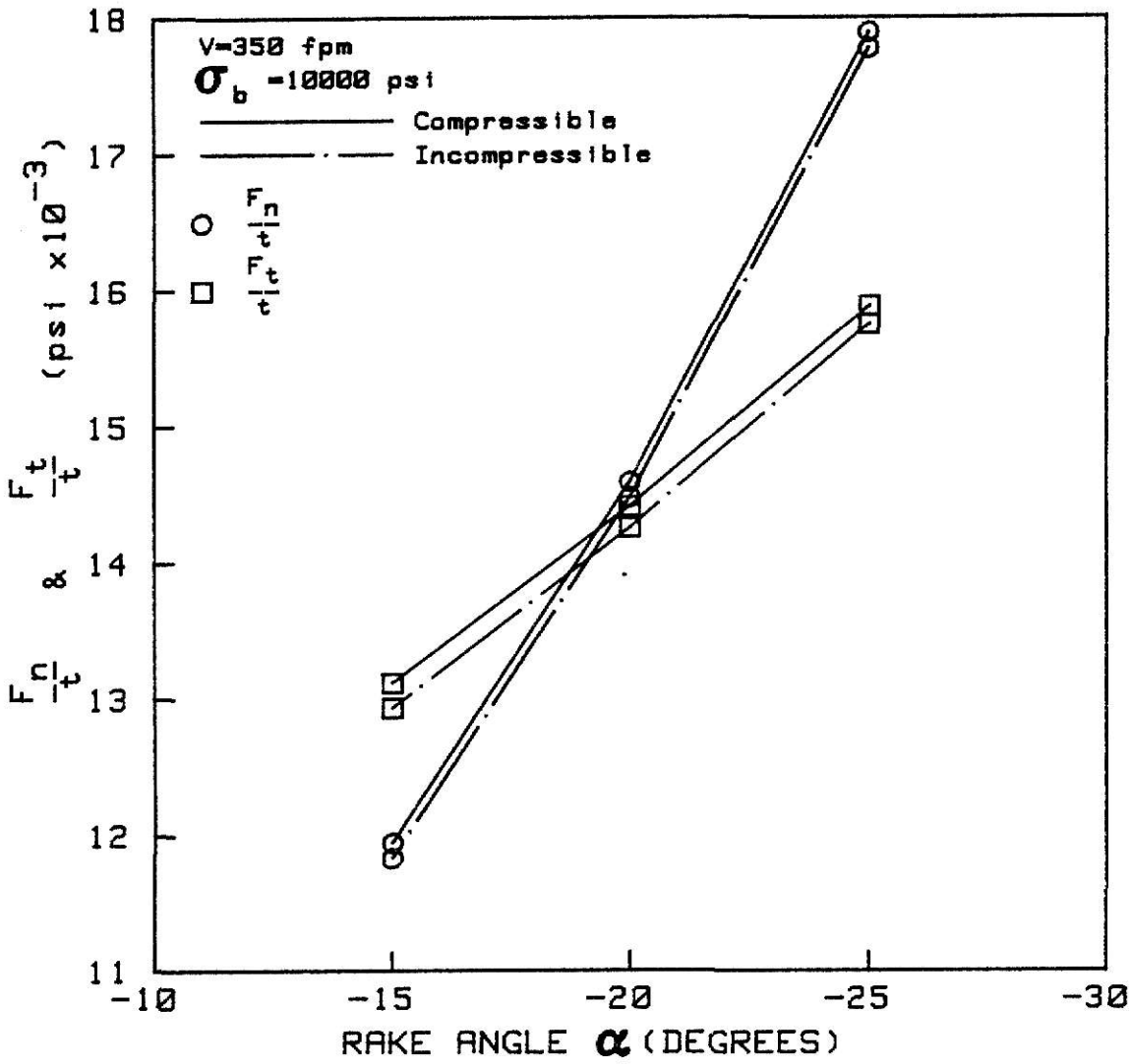

FIGURE 25 : THEORETICAL CUTTING FORCES FROM THE TWO PLASTICITY THEORIES FOR V = 350 fpm.

9.0 PRESSURE EFFECTS

9.1 Effect of Borehole Pressure

The borehole pressure σ_b changes the cutting forces considerably in rock cutting. The effects are analysed in this study. The other parameters remaining the same, an increase in borehole pressure **increases the cutting** forces.

Figure 26 shows the normal and tangential forces vs borehole pressure using the compressible theory solution. The numerical results are shown in Table 10 in Appendix III. The rake angle is -15 degrees, the pore pressure negligible and the area of the cutter 0.004 in^2.

It is evident from the graph that the normal and tangential forces increase with increase in borehole pressure. The possible reason for this effect is that an increase in borehole pressure makes the rock stronger and a larger cutting force is necessary to remove the rock material.

9.2 Effect of Pore Pressure

The fluids in the pores of the rock material tend to weaken the strength of the rock. The pressure created by the fluid affects the cutting process. The distribution of the pore pressure in the rock is not clearly understood. In the present analysis it is considered to be uniform. All the parameters remaining the same, an increase in pore pressure decreases the cutting forces.

Figure 27 gives the behaviour of the normal and tangential forces with respect to changes in the pore pressure. The corresponding numerical results are shown in Table 11 in Appendix III. The rake angle is -15 degrees,

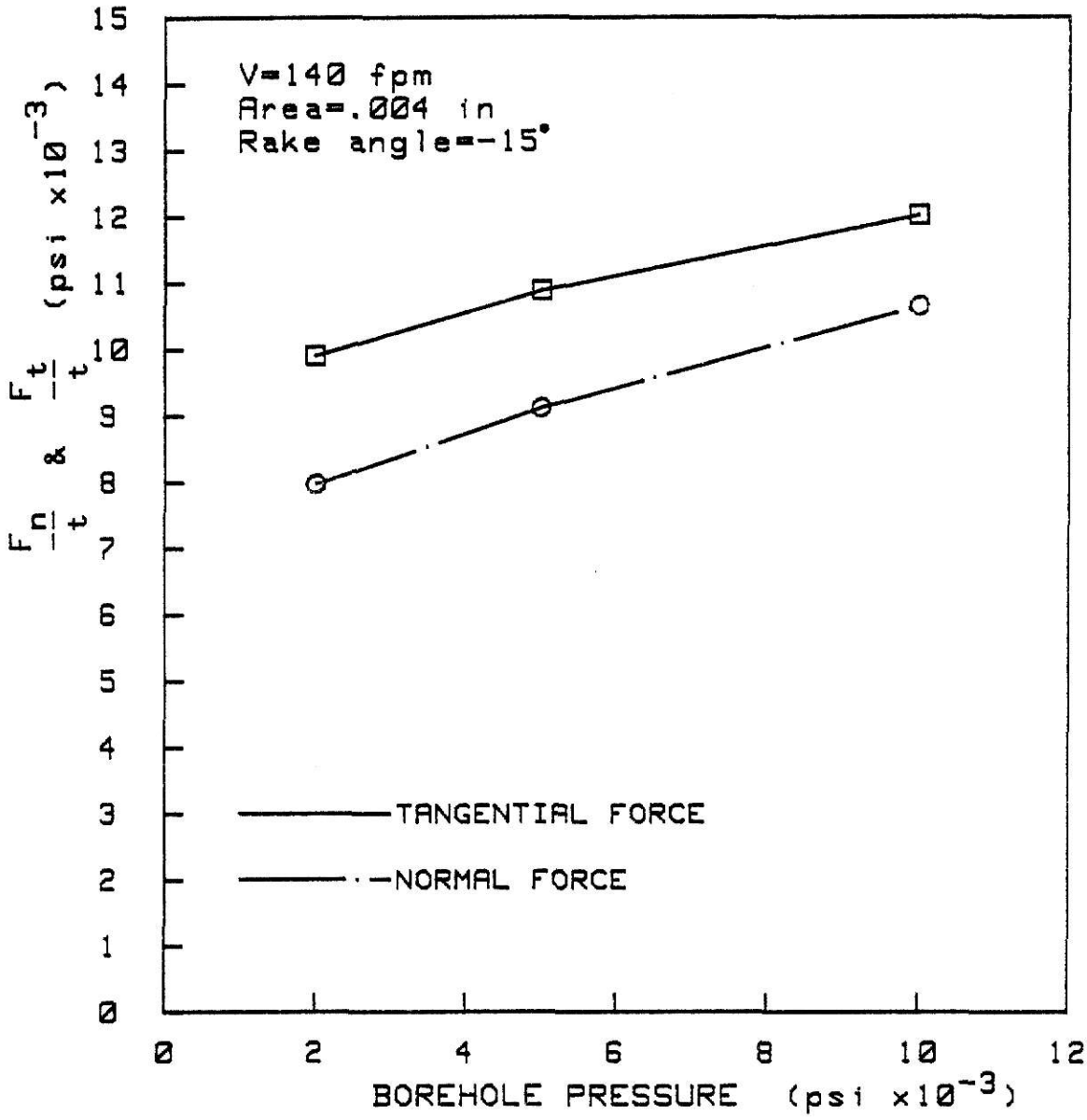

FIGURE 26 : CUTTING FORCE VARIATION WITH RESPECT TO THE BOREHOLE PRESSURE FOR α = -15°.

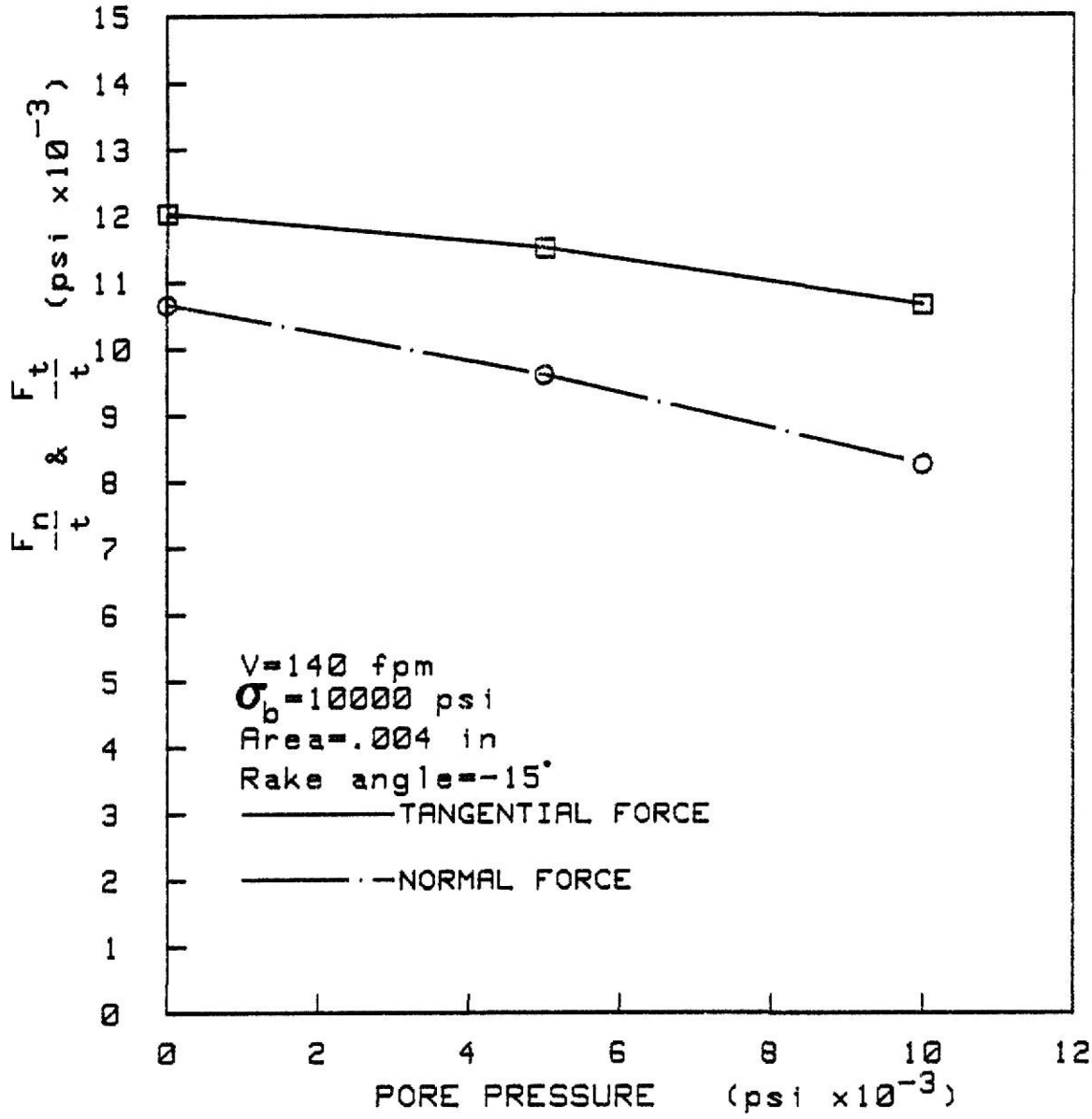

FIGURE 27 : CUTTING FORCE VARIATION WITH RESPECT TO THE PORE PRESSURE FOR α = -15°.

the borehole pressure 10000 psi and the cutter area 0.004 in^2. The velocity of the cutter is 140 fpm. The graph indicates that the cutting forces tend to decrease with increase in pore pressure. The reason is that the effective strength of the rock is decreased.

10.0 DISCUSSION AND CONCLUSION

The cutting theory developed in this study is the basis for a drilling theory for PDC oil well drill bits which can be used to develop improved bits. Even though the only material considered in the examples is Mancos Shale, the theory could be effectively used for other rock materials by changing the Mohr's envelope accordingly.

It is inferred from the results that for Mancos Shale, the two different plasticity theories namely the incompressible theory and the compressible theory, give similar values for the cutting forces. The main reason is that the Mohr's circle for the stress state is far from the origin where the slope of the Mohr's envelope is small. Hence the angle γ in the Mohr's circle is small and the maximum shear stress in the Mohr's circle is very nearly equal to the value of the shear stress at the point on the Mohr's circle at which the Mohr's envelope is a tangent. For other rock materials the results obtained from the two theories may differ more. The controlling factors are the position of the Mohr's circle with respect to the Mohr's envelope and the slope of the Mohr's envelope.

The differences in the experimental results of J.B. Cheatham [2] and J.F. Melaugh [1] are partially explained in this study. Since the velocity of the cutter was small in Cheatham's experiment the velocity effect has been neglected in the incompressible theory solution used to compare the results. The results obtained from the theory compared well with Cheatham's experimental results.

Melaugh conducted his experiments with much higher velocities. The

velocity effect incorporated in the solution has produced results which compare fairly well with the experimental results. The theoretical results might be better if the velocity effects were more completely understood. The normal force curves from the theoretical results are below the experimental results. One possible reason is that there is underflow below the cutter edge. This would cause increased normal force.

Material in the litreature [7, 8, 9] suggest that the yield strength of rocks increases with strain rate. Thus there is a possibility that the Mohr's envelope may become bigger when the velocity of the cutter increases. The theory would then fit the experimental curves better. Further study to obtain better understanding of velocity effects is recommended.

A theory for the friction magnitude between the tool and the rock material has not yet been developed. The friction magnitude has been determined by trial and error to fit the experimental curves as close as possible. Further work is required to develop an effective theory to properly predict the friction magnitude.

The pore pressure distribution has been assumed to be uniform in the rock. More work needs to be done to better understand the actual distribution of pore pressure in the rock.

REFERENCES

1. Salzer, J.A. and Melaugh, J.F., "Development of a Predictive Model for Drilling Pressurized Shale with STRATAPAX Blank Bits," paper presented at the ASME Energy Sources Technology Conference, Houston, January 18-22, 1981; available through Manager, Communications, Specialty Material Dept., General Electric Company, Worhington, Ohio.

2. Cheatham, J.B. Jr and Daniel, W.H., "A Study of Factors influencing the Drillability of Shale: Single Cutter Experiments with STRATAPAX Drill Blanks," paper presented at the ASME Energy Technology Conference and Exhibition, Houston, November 5-9, 1978; available through Manager, Communications, Specialty Materials Dept, General Electric Company, Worthington, Ohio.

3. Miller T.W. and Cheatham J.B. Jr., "Analytical Theory of Drilling," API project 67F, 1970-71.

4. Johnson W., Sowerby R. and Haddow J.B., Plane-Strain Slip-Line Fields: Theory and Bibliography, American Elsevier Publishing Company, Inc., New York, 1970.

5. Karafiath L.L. and Nowatzki E.A., Soil Mechanics for Off-Road Vehicle Engineering, Trans Tech Publications, Clausthal, Germany, 1978.

6. Jaeger J.C. and Cook N.G.W., Fundamentals of Rock Mechanics, Methuen & Co Ltd., 11, New Fetter Lane, London EC4, 1969.

7. Lankford J. Jr., "Dynamic Strength of Oil Shale," Society of Petroleum Engineers Journal, February, 1976.

8. Banton T.L., "Effect of Strain Rate from 10^{-2} to 10 sec^{-1} in Triaxial Compression tests on Three Rocks," International Journal of Rock Mechanics and Mining Science and Geo Mechanics Abstracts, Vol. 18, February 1981.

9. Chong K.P., Hoyt P.M., Smith J.W. and Paulsen , "Effects of Strain Rate on Oil Shale Fracturing," International Journal of Rock Mechanics and Mining Sciences and Geo Mechanics Abstracts, Vol. 17, February 1981.

APPENDIX I

Computer Program for the Incompressible Solution

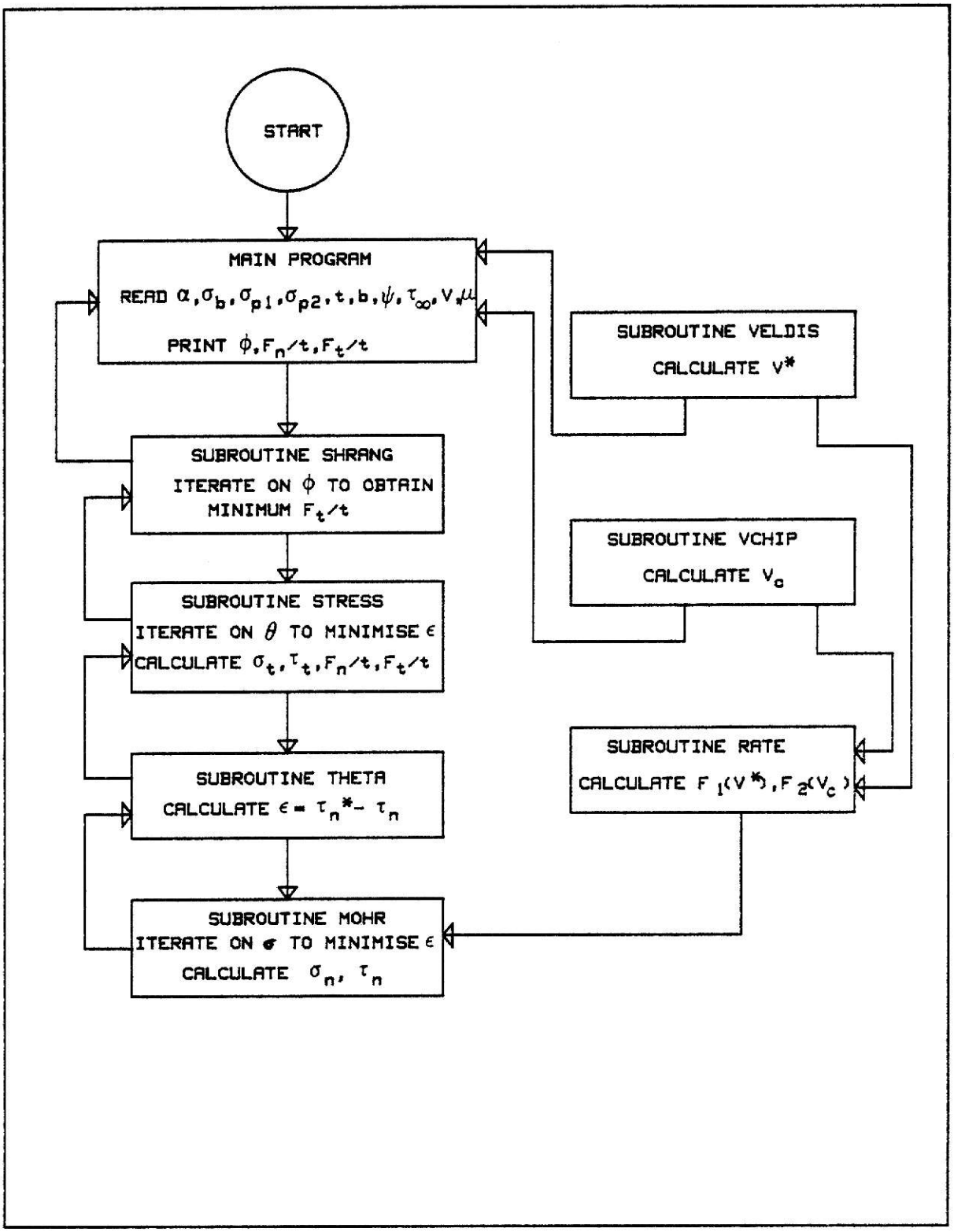

FIGURE 28 : FLOW CHART FOR THE INCOMPRESSIBLE SOLUTION.

```
C     ************************************************************
C     *                                                          *
C     *ROCK CUTTING THEORY FOR PDC CUTTERS-INCOMPRESSIBLE THEORY*
C     *                                                          *
C     ************************************************************
      IMPLICIT REAL*8(A-H,O-Z,$)
      REAL*8 NU
      COMMON T
      PI=3.14159265358979
      PIC=PI/180.00
      READ,T
      READ,B,TAUI,PSI,V,KSI,NU,SIGB,ALPD
      ALP=ALPD*PIC
      COSALP=DCOS(ALP)
      WRITE(6,50) V,ALPD,T
   50 FORMAT('0','V=',D15.8/'0','ALP=',D15.8/'0','T=',D15.8)
      WRITE (6,60) NU,TAUI,B,PSI
   60 FORMAT('0','NU=',D15.8/'0','TAUI=',D15.8/'0','B=',D15.8/
     X'0','PSI=',D15.8)
      READ,SIGP1,SIGP2
      CALL SHRANG(ALP,NU,TAUI,PSI,B,SIGB,V,PHI,SIGN,TAUN,FNOT,FT
     XOT,SIGP2,ISOL,SIGP1,SIGT,TAUT,I,J)
      CALL VELDIS(PHI,ALP,V,VDIS)
      CALL VCHIP(PHI,ALP,V,VC)
      WRITE(6,85) VDIS,VC
   85 FORMAT('0','VDIS=',F10.4/'0','VC=',F10.4)
      STOP
      END
C***************
C***************
      SUBROUTINE SHRANG(ALP,NU,TAUI,PSI,B,SIGB,V,PHI,SIGN,TAUN,
     XFNOT,FTOT,SIGP2,ISOL,SIGP1,SIGT,TAUT,I,J)
C
C     ******TO CALCULATE THE SHEAR ANGLE PHI********
C
      IMPLICIT REAL*8(A-H,O-Z,$)
      REAL*8 NU
      I=1
      TOL=5.D-3
      DPHI=0.01D0
      IDIR=1
      FR=1.D8
      PHILL=0.D0
      PHIRR=1.5707963Z+ALP
      PHI=0.D0
      IL=0
   20 PHI=PHI+DPHI
      IF(IDIR.EQ.1.AND.PHI.GE.PHIRR) PHI=0.5D0*(PHIL+PHIRR)
      IF(IDIR.EQ.-1.AND.PHI.LE.PHILL) PHI=0.5D0*(PHIRR+PHILL)
      CALL STRESS(PHI,ALP,NU,TAUI,PSI,B,SIGB,V,SIGN,TAUN,ISOL,
     XSIGP2,SIGP1,FTOT,FNOT,SIGT,THA,I)
      IF(ISOL.EQ.4) GO TO 100
```

```
      IF(I.GT.2.AND.IL.EQ.2) GO TO 30
      I=I+1
      IF(IL.EQ.1) GO TO 25
      IL=1
      PHILL=PHI
      GO TO 20
   25 IL=2
      FL=FTOT
      PHIL=PHI
      DPHI=0.1D0
      GO TO 20
   30 IF(IDIR.EQ.1.AND.FTOT.GT.FL) GO TO 40
      IF(IDIR.EQ.-1.AND.FTOT.GT.FR) GO TO 40
      IF(IDIR.EQ.-1) GO TO 35
      PHILL=PHIL
      FL=FTOT
      PHIL=PHI
      GO TO 20
   35 CONTINUE
      PHIRR=PHIR
      FR=FTOT
      PHIR=PHI
      GO TO 20
   40 CONTINUE
      IF(IDIR.EQ.1.AND.(PHI-PHILL)/(PHI+PHILL).LT.TOL) GO TO 60
      IF(IDIR.EQ.-1.AND.(PHIRR-PHI)/(PHIRR+PHI).LT.TOL) GO TO 60
      IF(IDIR.EQ.-1) GO TO 50
      PHIRR=PHI
      FR=FTOT
      PHIR=PHI
      IDIR=-IDIR
      DPHI=-0.2D0*(PHIRR-PHILL)
      GO TO 20
   50 CONTINUE
      PHILL=PHI
      FL=FTOT
      PHIL=PHI
      IDIR=-IDIR
      DPHI=0.2D0*(PHIRR-PHILL)
      GO TO 20
   60 CONTINUE
      IF(IDIR.EQ.1) PHI=0.5D0*(PHILL+PHI)
      IF(IDIR.EQ.-1) PHI=0.5D0*(PHIRR+PHI)
      CALL STRESS(PHI,ALP,NU,TAUI,PSI,B,SIGB,V,SIGN,TAUN,ISOL,
     XSIGP2,SIGP1,FTOT,FNOT,SIGT,THA,I)
      WRITE(6,200) PHI,FTOT,FNOT,SIGN,SIGT,TAUN,TAUT,SIGB,SIGP1,
     XSIGP2,THA
  200 FORMAT('0','PHI=',F12.7/'0','FTOT=',F10.2/'0','FNOT=',F10.2
     X/'0','SIGN=',D15.8/'0','SIGT=',D15.8/'0','TAUN=',D15.8/
     X'0','TAUT=',D15.8/'0','SIGB=',D15.8/'0','SIGP1=',D15.8/
     X'0','SIGP2=',D15.8/'0','THETA=',F12.7)
      RETURN
```

```
  100 DPHI=0.1D0
      GO TO 20
      END
C***************
C***************
      SUB ROUTINE STRESS(PHI,ALP,NU,TAUI,PSI,B,SIGB,V,SIGN,TAUN,
     XISCL,SIGP2,SIGP1,FTOT,FNCT,SIGT,TAUT,THA,I)
C
C      ********TO CALCULATE THE ANGLE THETA*********
C
      IMPLICIT REAL*8(A-H,O-Z,$)
      REAL*8 NU
      COMMON T
      I=1
      TOL=1.D-6
      ITIR=1
      DTHA=0.01D0
      THARR=1.57070796+PHI-ALP
      THAMAX=1.57070796+PHI-ALP
      THALL=PHI
      THA=0.0D0
      IL=0
   10 THA=THA+DTHA
      IF(THA.GE.THAMAX) GO TO 15
      CALL THETA(PHI,ALP,THA,NU,TAUI,PSI,B,SIGB,V,SIGN,TAUN,ISCL
     X,SIGP2,SIGP1,FTOT,FNCT,SIGT,TAUT,DIF,TAUSTR)
      IF(I.GT.2.AND.IL.EQ.2) GO TO 35
      I=I+1
      IF(IL.EQ.1) GO TO 25
      IL=1
      THALL=THA
      GO TO 10
   25 IL=2
      DIFL=DIF
      THAL=THA
      DTHA=0.01D0
      GO TO 10
   35 IF(DIFL.GT.0.D0.AND.DIF.LT.0.D0) GO TO 55
      DIFL=DIF
      THALL=THAL
      THAL=THA
      DTHA=0.01D0
      GO TO 10
   55 IF(TAUSTR.LT.0.D0.OR.TAUN.LT.0.D0) GO TO 10
      THALL=THAL
      THARR=THA
      DIFR=DIF
   60 THANW=((THARR-THALL)*(-DIFL)/(DIFR-DIFL))+THALL
      THA=THANW
      CALL THETA(PHI,ALP,THA,NU,TAUI,PSI,B,SIGB,V,SIGN,TAUN,ISCL
     X,SIGP2,SIGP1,FTOT,FNCT,SIGT,TAUT,DIF,TAUSTR)
      IF(DIF.LT.0.D0) GO TO 65
```

```
      IF(DIF.GT.0.D0) GO TO 75
   65 IF(((THA-THALL)/(THA+THALL)).LT.TOL) GO TO 85
      THARR=THA
      DIFR=DIF
      GO TO 60
   75 IF(((THARR-THA)/(THARR+THA)).LT.TOL) GO TO 85
      THALL=THA
      DIFL=DIF
      GO TO 60
   85 CONTINUE
      IF(DIF.LT.0.D0) THA=0.5D0*(THALL+THA)
      IF(DIF.GT.0.D0) THA=0.5D0*(THARR+THA)
      CALL THETA(PHI,ALP,THA,NU,TAUI,PSI,B,SIGB,V,SIGN,TAUN,ISOL
     X,SIGP2,SIGP1,FTOT,FNOT,SIGT,TAUT,DIF,TAUSTR)
      SINPMA=DSIN(PHI-ALP)
      COSPMA=DCOS(PHI-ALP)
      TANPMA=DTAN(PHI-ALP)
      TANPMT=DTAN(THA-PHI+ALP)
      COSPMT=DCOS(THA-PHI+ALP)
      SINPMT=DSIN(THA-PHI+ALP)
      A2OA1=SINPMA+TANPMT*COSPMA
      A3OA1=COSPMA/COSPMT
      A2OA3=COSPMT*TANPMA+SINPMT
      COSTH=DCOS(THA)
      SINTH=DSIN(THA)
      A1=T/DSIN(PHI)
      A2=A2OA1*A1
      A3=A3OA1*A1
C
C     ******TO SATISFY EQULIBRIUM**********
C
      SUMY=SIGN*A1-A2*TAUT*COSPMA-SIGT*A2*SINPMA-SIGB*A3*COSTH
      SUMX=TAUN*A1+A2*TAUT*SINPMA-SIGT*A2*COSPMA+SIGB*A3*SINTH
      AMOMD=SIGB*A3*(A3/2.D0-A1*COSTH/2.D0)-SIGT*A2*(A2/2.D0-
     XA1*SINPMA/2.D0)+TAUT*A2*A1*COSPMA/2.D0
C
C     **********TO CALCULATE THE CUTTING FORCES**********
C
      FNOT=((SIGB-SIGT)*DSIN(ALP)+NU*(SIGT-SIGP2)*DCOS(ALP))*
     XA2OA1/DSIN(PHI)
      FTOT=((SIGT-SIGB)*DCOS(ALP)+NU*(SIGT-SIGP2)*DSIN(ALP))*
     XA2OA1/DSIN(PHI)
      WRITE(6,40) SUMX,SUMY,AMOMD
   40 FORMAT('0',D15.8,5X,D15.8,5X,D15.8)
      RETURN
   15 ISOL=4
      WRITE(6,16) ISOL
   16 FORMAT('0','ISOL=',I4)
      GO TO 100
  100 RETURN
      END
C*************
```

```
C*************
      SUB ROUTINE THETA(PHI,ALP,THA,NU,TAUI,PSI,B,SIGB,V,SIGN,
     XTAUN,ISOL,SIGP2,SIGP1,FTCT,FNOT,SIGT,TAUT,DIF,TAUSTR)
C
C     ***TO CALCULATE THE DIFFERENCE BETWEEN TAUN AND TAUSTR**
C
      IMPLICIT REAL*8(A-H,O-Z,$)
      REAL*8 NU
      POROS=0.2D0
      FAC=POROS**(2.D0/3.D0)
      SINPMA=DSIN(PHI-ALP)
      COSPMA=DCOS(PHI-ALP)
      TANPMA=DTAN(PHI-ALP)
      TANPMT=DTAN(THA-PHI+ALP)
      COSPMT=DCOS(THA-PHI+ALP)
      SINPMT=DSIN(THA-PHI+ALP)
      A20A1=SINPMA+TANPMT*COSPMA
      A30A1=COSPMA/COSPMT
      A20A3=COSPMT*TANPMA+SINPMT
      COSTH=DCOS(THA)
      SINTH=DSIN(THA)
      ISOL=1
      COSBR=A30A1-COSTH
      ANRSGT=(SIGB*A30A1*COSBR)-(NU*FAC*SIGP2*A20A1*COSPMA)
      DRSGT=A20A1*(A20A1-SINPMA-NU*COSPMA)
      SIGT=ANRSGT/DRSGT
      TAUT=NU*(SIGT-FAC*SIGP2)
      SIGN=A20A1*TAUT*COSPMA+A20A1*SIGT*SINPMA+A30A1*SIGB*COSTH
      CALL MOHR(PHI,ALP,THA,TAUI,PSI,B,SIGB,V,SIGN,TAUN,SIGP2,
     XSIGP1,ISOL)
      TAUSTR=A20A1*SIGT*COSPMA-A20A1*TAUT*SINPMA-SIGB*A30A1*SINTH
      DIF=TAUSTR-TAUN
      RETURN
      END
C**************
C**************
      SUB ROUTINE MOHR(PHI,ALP,THA,TAUI,PSI,B,SIGB,V,SIGN,TAUN,
     XSIGP2,SIGP1,ISOL)
C
C     *******TO FIT THE MOHR'S ENVELOPE***********
C
      IMPLICIT REAL*8(A-H,O-Z,$)
      REAL*8 NU
      TOL=5.D-3
      ETA=1.D0
      CALL RATE(PHI,ALP,V,F1,F2)
      SIG=SIGB
      SIGO=SIG
      EXP=DEXP(-PSI*SIGO)
      TAU=TAUI-B*EXP
      TANG=B*EXP*PSI
      GAM=DATAN(TANG)
```

```
      SING=DSIN(GAM)
      COSG=DCOS(GAM)
      TAUN=TAU/COSG+F1
      SGNSTR=SIGP1+SIGO+TAU*TANG
      EPS=SGNSTR-SIGN
      DTAU=PSI*B*EXP
      D2TAU=-PSI*DTAU
      DGAM=D2TAU*COSG*COSG
      D2GAM=-DGAM*PSI+2.D0*(-D2TAU)*COSG*SING*DGAM
      DEPS=1.D0+DTAU*TANG+TAU*DGAM/COSG**2
      D2EPS=+D2TAU*TANG+2.D0*DTAU*DGAM/COSG**2+TAU*D2GAM/COSG
     X**2+2.D0*TAU*SING*DGAM*DGAM/COSG**3
      SIG=SIGO
      ARG=DEPS**2-2.D0*DEPS*EPS
      IF(ARG.GT.0.D0) SIG=SIG+(-DEPS-DSQRT(ARG))/D2EPS
   10 CONTINUE
      X=-PSI*SIG
      IF(X.GT.70.D0) X=70.D0
      IF(X.LT.-70.D0) X=-70.D0
      EXP=DEXP(X)
      TAU=TAUI-B*EXP
      TANG=B*EXP*PSI
      GAM=DATAN(TANG)
      SING=DSIN(GAM)
      COSG=DCOS(GAM)
      TAUN=TAU/COSG+F1
      SGNSTR=SIGP1+SIG+TAU*TANG
      EPS=SGNSTR-SIGN
      DTAU=PSI*B*EXP
      D2TAU=-PSI*DTAU
      DGAM=D2TAU*COSG*COSG
      DEPS=1.D0+DTAU*TANG+TAU*DGAM/COSG**2
      SIG2=SIG-ETA*EPS/DEPS
      IF((DABS(SIG2-SIG)/TAU).LT.TOL) GO TO 20
      SIG=SIG2
      GO TO 10
   20 CONTINUE
      RETURN
      END
C*********************
C*********************
      SUB ROUTINE VCHIP(PHI,ALP,V,VC)
C
C     *********TO CALCULATE THE CHIP VELOCITY***********
C
      IMPLICIT REAL*8(A-H,O-Z,$)
      VC=V*DSIN(PHI)/DCOS(PHI-ALP)
      RETURN
      END
C*********************
```

```
C***************
      SUB ROUTINE VELDIS(PHI,ALP,V,VDIS)
C
C     *********TO CALCULATE THE VELOCITY DISCONTINUITY*******
C
      IMPLICIT REAL*8(A-H,C-Z,$)
      VDIS=V*DCOS(ALP)/DCOS(PHI-ALP)
      RETURN
      END
C*****************
C*****************
      SUB ROUTINE RATE(PHI,ALP,V,F1,F2)
C
C     *******TO CALCULATE THE VELOCITY EFFECTS**********
C
      IMPLICIT REAL*8(A-H,O-Z,$)
      A=0.4D0
      CALL VCHIP(PHI,ALP,V,VC)
      F2=A*VC
      CALL VELDIS(PHI,ALP,V,VDIS)
      F1=A*VDIS
      RETURN
      END
```

APPENDIX II

Computer Program for the Compressible Solution

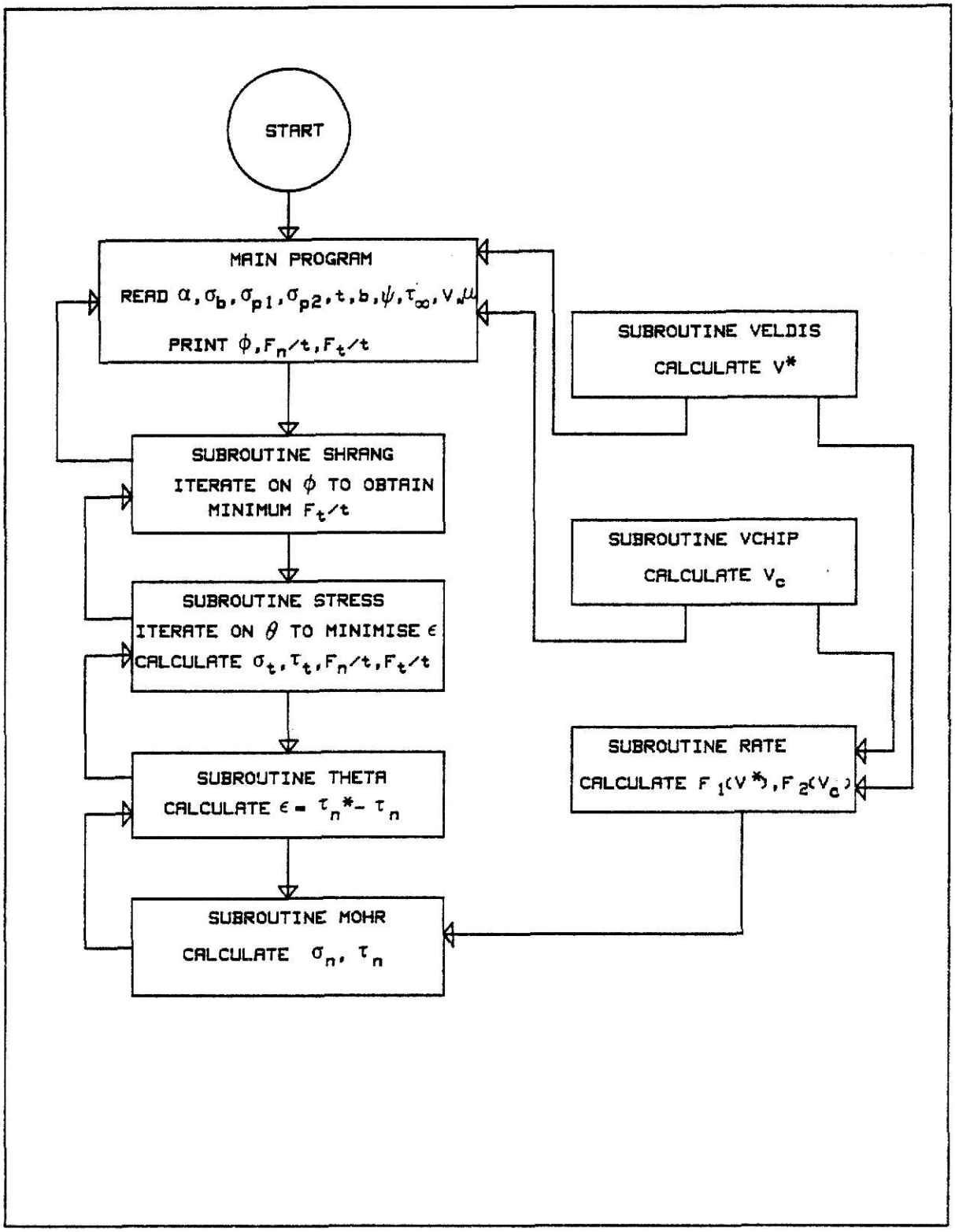

FIGURE 29 : FLOW CHART FOR THE COMPRESSIBLE SOLUTION.

```
C     ************************************************************
C     *                                                          *
C     *ROCK CUTTING THEORY FOR PDC CUTTERS-COMPRESSIBLE THEORY   *
C     *                                                          *
C     ************************************************************
      IMPLICIT REAL*8(A-H,O-Z,$)
      REAL*8 NU
      COMMON T
      PI=3.14159265358979
      PIC=PI/180.00
      READ,T
      READ,B,TAUI,PSI,V,KSI,NU,SIGB,ALPD
      ALP=ALPD*PIC
      COSALP=DCOS(ALP)
      WRITE(6,50) V,ALPD,T
   50 FORMAT('0','V=',D15.8/'0','ALP=',D15.8/'0','T=',D15.8)
      WRITE (6,60) NU,TAUI,B,PSI
   60 FORMAT('0','NU=',D15.8/'0','TAUI=',D15.8/'0','B=',D15.8/
     X'0','PSI=',D15.8)
      READ,SIGP1,SIGP2
      CALL SHRANG(ALP,NU,TAUI,PSI,B,SIGB,V,PHI,SIGN,TAUN,FNOT
     X,ISOL,SIGP1,SIGT,TAUT,I,J,VDIS,VC,GAM,F1,FTOT,SIGP2)
      WRITE(6,85) VDIS,VC
   85 FORMAT('0','VDIS=',F10.4/'0','VC=',F10.4)
      STOP
      END
C***************
C***************
      SUBROUTINE SHRANG(ALP,NU,TAUI,PSI,B,SIGB,V,PHI,SIGN,TAU
     XN,FNOT,ISOL,SIGP1,SIGT,TAUT,I,J,VDIS,VC,GAM,F1,FTOT,SIGP2)
C
C     ******TO CALCULATE THE SHEAR ANGLE PHI********
C
      IMPLICIT REAL*8(A-H,O-Z,$)
      REAL*8 NU
      I=1
      TOL=5.D-3
      DPHI=0.01D0
      IDIR=1
      FR=1.D8
      PHILL=0.DO
      PHIRR=1.57079632+ALP
      PHI=0.0DO
      IL=0
   20 PHI=PHI+DPHI
      IF(IDIR.EQ.1.AND.PHI.GE.PHIRR) PHI=0.5DO*(PHIL+PHIRR)
      IF(IDIR.EQ.-1.AND.PHI.LE.PHILL) PHI=0.5DO*(PHIR+PHILL)
      CALL STRESS(PHI,ALP,NU,TAUI,PSI,B,SIGB,V,SIGN,TAUN,ISOL,
     XSIGP2,SIGP1,FTOT,FNOT,SIGT,TAUT,THA,I,VDIS,VC,GAM,F1)
      IF(ISOL.EQ.4) GO TO 100
      IF(I.GT.2.AND.IL.EQ.2) GO TO 30
      I=I+1
```

```
      IF(IL.EQ.1) GO TO 25
      IL=1
      PHILL=PHI
      GO TO 20
   25 IL=2
      FL=FTOT
      PHIL=PHI
      DPHI=0.1D0
      GO TO 20
   30 IF(IDIR.EQ.1.AND.FTOT.GT.FL) GO TO 40
      IF(IDIR.EQ.-1.AND.FTOT.GT.FR) GO TO 40
      IF(IDIR.EQ.-1) GO TO 35
      PHILL=PHIL
      FL=FTOT
      PHIL=PHI
      GO TO 20
   35 CONTINUE
      PHIRR=PHIR
      FR=FTOT
      PHIR=PHI
      GO TO 20
   40 CONTINUE
      IF(IDIR.EQ.1.AND.(PHI-PHILL)/(PHI+PHILL).LT.TOL) GO TO 60
      IF(IDIR.EQ.-1.AND.(PHIRR-PHI)/(PHIRR+PHI).LT.TOL) GO TO 60
      IF(IDIR.EQ.-1) GO TO 50
      PHIRR=PHI
      FR=FTOT
      PHIR=PHI
      IDIR=-IDIR
      DPHI=-0.2D0*(PHIRR-PHILL)
      GO TO 20
   50 CONTINUE
      PHILL=PHI
      FL=FTOT
      PHIL=PHI
      IDIR=-IDIR
      DPHI=0.2D0*(PHIRR-PHILL)
      GO TO 20
   60 CONTINUE
      IF(IDIR.EQ.1) PHI=0.5D0*(PHILL+PHI)
      IF(IDIR.EQ.-1) PHI=0.5D0*(PHIRR+PHI)
      CALL STRESS(PHI,ALP,NU,TAUI,PSI,B,SIGB,V,SIGN,TAUN,ISOL,
     XSIGP2,SIGP1,FTOT,FNOT,SIGT,TAUT,THA,I,VDIS,VC,GAM,FI)
      WRITE(6,200) PHI,FTOT,FNOT,SIGN,SIGT,TAUN,TAUT,SIGB,SIGP1,
     XSIGP2,THA
  200 FORMAT('0','PHI=',F12.7/'0','FTOT=',F10.2/'0','FNOT=',F10.2
     X/'0','SIGN=',D15.8/'0','SIGT=',D15.8/'0','TAUN=',D15.8/
     X'0','TAUT=',D15.8/'0','SIGB=',D15.8/'0','SIGP1=',D15.8/
     X'0','SIGP2=',D15.8/'0','THETA=',F12.7)
      RETURN
  100 DPHI=0.1D0
      GO TO 20
```

```
      END
C**************
C**************
      SUB ROUTINE STRESS(PHI,ALP,NU,TAUI,PSI,B,SIGB,V,SIGN,TAUN
     X,ISOL,SIGP2,SIGP1,FTOT,FNOT,SIGT,TAUT,THA,I,VDIS,VC,GAM,F1)
C
C     ********TO CALCULATE THE ANGLE THETA*********
C
      IMPLICIT REAL*8(A-H,O-Z,$)
      COMMON T
      REAL*8 NU
      I=1
      TOL=5.D-5
      ITIR=1
      DTHA=0.01D0
      THARR=1.57070796+PHI-ALP
      THAMAX=1.57070796+PHI-ALP
      THALL=PHI
      THA=0.D0
      IL=0
   10 THA=THA+DTHA
      IF(THA.GE.THAMAX) GO TO 15
      CALL THETA(PHI,ALP,THA,NU,TAUI,PSI,B,SIGB,V,SIGN,TAUN,ISOL
     X,SIGP1,SIGP2,FTOT,FNOT,SIGT,TAUT,DIF,TAUSTR,VDIS,VC,GAM,F1)
      IF(I.GT.2.AND.IL.EQ.2) GO TO 35
      I=I+1
      IF(IL.EQ.1) GO TO 25
      IL=1
      THALL=THA
      GO TO 10
   25 IL=2
      DIFL=DIF
      THAL=THA
      DTHA=0.01D0
      GO TO 10
   35 IF(DIFL.GT.0.D0.AND.DIF.LT.0.D0) GO TO 55
      DIFL=DIF
      THALL=THAL
      THAL=THA
      DTHA=0.01D0
      GO TO 10
   55 IF(TAUSTR.LT.0.D0.OR.TAUN.LT.0.D0) GO TO 10
      THALL=THAL
      THARR=THA
      DIFR=DIF
   60 THANW=((THARR-THALL)*(-DIFL)/(DIFR-DIFL))+THALL
      THA=THANW
      CALL THETA(PHI,ALP,THA,NU,TAUI,PSI,B,SIGB,V,SIGN,TAUN,ISOL
     X,SIGP1,SIGP2,FTOT,FNOT,SIGT,TAUT,DIF,TAUSTR,VDIS,VC,GAM,F1)
      IF(DIF.LT.0.D0) GO TO 65
      IF(DIF.GT.0.D0) GO TO 75
   65 IF(((THA-THALL)/(THA+THALL)).LT.TOL) GO TO 85
```

```
      THARR=THA
      DIFR=DIF
      GO TO 60
   75 IF(((THARR-THA)/(THARR+THA)).LT.TOL) GO TO 85
      THALL=THA
      DIFL=DIF
      GO TO 60
   85 CONTINUE
      IF(DIF.LT.0.D0) THA=0.5D0*(THALL+THA)
      IF(DIF.GT.0.D0) THA=0.5D0*(THARR+THA)
      CALL THETA(PHI,ALP,THA,NU,TAUI,PSI,B,SIGB,V,SIGN,TAUN,ISOL
     X,SIGP1,SIGP2,FTOT,FNOT,SIGT,TAUT,DIF,TAUSTR,VDIS,VC,GAM,FI)
      SINPMA=DSIN(PHI-ALP)
      COSPMA=DCOS(PHI-ALP)
      TANPMA=DTAN(PHI-ALP)
      TANPMT=DTAN(THA-PHI+ALP)
      COSPMT=DCOS(THA-PHI+ALP)
      SINPMT=DSIN(THA-PHI+ALP)
      A2OA1=SINPMA+TANPMT*COSPMA
      A3OA1=COSPMA/COSPMT
      A2OA3=COSPMT*TANPMA+SINPMT
      COSTH=DCOS(THA)
      SINTH=DSIN(THA)
      A1=T/DSIN(PHI)
      A2=A2OA1*A1
      A3=A3OA1*A1
C
C     ******TO SATISFY EQULIBRIUM**********
C
      SUMY=SIGN*A1-A2*TAUT*COSPMA-SIGT*A2*SINPMA-SIGB*A3*COSTH
      SUMX=TAUN*A1+A2*TAUT*SINPMA-SIGT*A2*COSPMA+SIGB*A3*SINTH
      AMOMD=SIGB*A3*(A3/2.D0-A1*COSTH/2.D0)-SIGT*A2*(A2/2.D0-A1*
     XSINPMA/2.D0)+TAUT*A2*A1*COSPMA/2.D0
C
C     **********TO CALCULATE THE CUTTING FORCES**********
C
      FNOT=((SIGB-SIGT)*DSIN(ALP)+NU*(SIGT-SIGP2)*DCOS(ALP))*
     XA2OA1/DSIN(PHI)
      FTOT=((SIGT-SIGB)*DCOS(ALP)+NU*(SIGT-SIGP2)*DSIN(ALP))*
     XA2OA1/DSIN(PHI)
      WRITE(6,40) SUMX,SUMY,AMOMD
   40 FORMAT('0',D15.8,5X,D15.8,5X,D15.8)
      RETURN
   15 ISOL=4
      WRITE(6,16) ISOL
   16 FORMAT('0','ISOL=',F7.2)
      GO TO 100
  100 RETURN
      END
C**********
C**********
```

```
      SUB ROUTINE THETA(PHI,ALP,THA,NU,TAUI,PSI,B,SIGB,V,SIGN,
     XTAUN,ISOL,SIGP1,SIGP2,FTOT,FNOT,SIGT,TAUT,DIF,TAUSTR,VDIS,
     XVC,GAM,F1)
C
C      ****TO CALCULATE THE DIFFERENCE BETWEEN TAUN AND TAUSTR***
C
      IMPLICIT REAL*8(A-H,O-Z,$)
      REAL*8 NU
      POROS=0.2D0
      FAC=POROS**(2.D0/3.D0)
      SINPMA=DSIN(PHI-ALP)
      COSPMA=DCOS(PHI-ALP)
      TANPMA=DTAN(PHI-ALP)
      TANPMT=DTAN(THA-PHI+ALP)
      COSPMT=DCOS(THA-PHI+ALP)
      SINPMT=DSIN(THA-PHI+ALP)
      A2OA1=SINPMA+TANPMT*COSPMA
      A3OA1=COSPMA/COSPMT
      A2OA3=COSPMT*TANPMA+SINPMT
      COSTH=DCOS(THA)
      SINTH=DSIN(THA)
      ISOL=1
      COSBR=A3OA1-COSTH
      ANRSGT=(SIGB*A3OA1*COSBR)-(NU*FAC*SIGP2*A2OA1*COSPMA)
      DRSGT=A2OA1*(A2OA1-SINPMA-NU*COSPMA)
      SIGT=ANRSGT/DRSGT
      TAUT=NU*(SIGT-FAC*SIGP2)
      SIGN=A2OA1*TAUT*COSPMA+A2OA1*SIGT*SINPMA+A3OA1*SIGB*COSTH
      CALL MOHR(PHI,ALP,THA,TAUI,PSI,B,SIGB,V,SIGN,TAUN,SIGP2,
     XSIGP1,ISOL,VDIS,VC,F1,GAM)
      TAUSTR=A2OA1*SIGT*COSPMA-A2OA1*TAUT*SINPMA-SIGB*A3OA1*SINTH
      DIF=TAUSTR-TAUN
      RETURN
      END
C**************
C**************
      SUB ROUTINE MOHR(PHI,ALP,THA,TAUI,PSI,B,SIGB,V,SIGN,TAUN,
     XSIGP2,SIGP1,ISOL,VDIS,VC,F1,GAM)
C
C      **********TO CALCULATE SIGN AND TAUN***********
C
      IMPLICIT REAL*8(A-H,O-Z,$)
      REAL*8 NU
      X=-PSI*(SIGN-SIGP1)
      IF(X.GT.70.D0)X=70.D0
      IF(X.LT.-70.D0) X=-70.D0
      EXP=DEXP(X)
      TANGAM=B*PSI*EXP
      GAM=DATAN(TANGAM)
      CALL VELDIS(PHI,ALP,GAM,V,VDIS)
      CALL VCHIP(PHI,ALP,GAM,V,VC)
      CALL RATE(VDIS,F1)
```

```
      TAUN=TAUI+F1-B*EXP
      RETURN
      END
      SUB ROUTINE VELDIS(PHI,ALP,GAM,V,VDIS)
C
C     **********TO CALCULATE THE VELOCITY DISCONTINUITY*******
C
      IMPLICIT REAL*8(A-H,O-Z,$)
      VDIS=DCOS(ALP)*V/DCOS(PHI-ALP+GAM)
      RETURN
      END
C************
C************
      SUB ROUTINE VCHIP(PHI,ALP,GAM,V,VC)
C
C     **********TO CALCULATE THE CHIP VELOCITY************
C
      IMPLICIT REAL*8(A-H,O-Z,$)
      VC=DSIN(PHI+GAM)*V/DCOS(PHI-ALP+GAM)
      RETURN
      END
C*************
C*************
      SUB ROUTINE RATE(VDIS,F1)
C
C     *******TO CALCULATE THE VELOCITY EFFECTS*********
C
      IMPLICIT REAL*8(A-H,O-Z,$)
      A=0.4DO
      F1=A*VDIS
      RETURN
      END
```

APPENDIX III

Numerical Results

TABLE 2: THEORETICAL RESULTS FOR VELOCITY OF 140 fpm
USING INCOMPRESSIBLE THEORY SOLUTION.

BOREHOLE PRESSURE=10000 psi VELOCITY EFFECTS: $F_1(V^*)=0.4$ $F_2(V_c)=1.4$

RAKE ANGLE α (Degrees)	-25	-20	-15	-10
FRICTION FACTOR μ	0.35	0.39	0.42	0.43
TANGENTIAL FORCE PER UNIT AREA F_t/t (psi)	142014	130841	118560	103835
NORMAL FORCE PER UNIT AREA F_n/t (psi)	152359	129009	105573	80540
NORMAL STRESS ON THE SHEAR PLANE σ_n (psi)	72858	66831	60150	52024
SHEAR STRESS ON THE SHEAR PLANE τ_n (psi)	27642	26966	26062	24686
NORMAL STRESS ON THE RAKE FACE σ_t (psi)	74475	67565	60850	54231
SHEAR STRESS ON THE RAKE FACE τ_t (psi)	27065	26349	25556	23319
SHEAR ANGLE ϕ (Degrees)	19.25	20.02	20.86	21.77
ANGLE θ (Degrees)	66.26	64.61	62.54	59.57
VELOCITY DISCONTINUITY V^* (ipm)	2125.62	2061.42	2002.18	1946.07
VELOCITY OF THE CHIP V_c (ipm)	773.23	751.00	737.95	732.92

TABLE 3 : THEORETICAL RESULTS FOR VELOCITY OF 350 fpm
USING INCOMPRESSIBLE THEORY SOLUTION..

BOREHOLE PRESSURE=10000 psi. VELOCITY EFFECTS: $F_1(V^*)$= 0.4 F_2 (V_c) =1.4

RAKE ANGLE α (Degrees)	-25	-20	-15	-10
FRICTION FACTOR μ	0.38	0.41	0.44	0.46
TANGENTIAL FORCE PER UNIT AREA F_t/t (psi)	157510	142598	129322	115541
NORMAL FORCE PER UNIT AREA F_n/t (psi)	177747	144817	118318	93602
NORMAL STRESS ON THE SHEAR PLANE σ_n (psi)	81534	73293	66189	58625
SHEAR STRESS ON THE SHEAR PLANE τ_n (psi)	29653	28895	28071	26983
NORMAL STRESS ON THE RAKE FACE σ_t (psi)	80546	72369	65287	58639
SHEAR STRESS ON THE RAKE FACE τ_t (psi)	30606	29671	28726	26974
SHEAR ANGLE ϕ (Degrees)	19.03	20.02	21.00	21.96
ANGLE θ (Degrees)	67.49	65.46	63.45	60.97
VELOCITY DISCONTINUITY V^* (ipm)	5294.28	5153.54	5014.51	4875.25
VELOCITY OF THE CHIP V_c (ipm)	1904.68	1877.50	1860.32	1851.37

TABLE 4: THEORETICAL RESULTS FOR THE TWO THEORIES.

RAKE ANGLE=-25° FRICTION COEFFICIENT=0.35

BOREHOLE PRESSURE=10000 psi VELOCITY OF CUTTER=140 fpm

	COMPRESSIBLE	INCOMPRESSIBLE
TANGENTIAL FORCE PER UNIT AREA F_t/t (psi)	143192	142014
NORMAL FORCE PER UNIT AREA F_n/t (psi)	153289	152359
NORMAL STRESS ON THE SHEAR PLANE σ_n (psi)	74587	72857
SHEAR STRESS ON THE SHEAR PLANE τ_n (psi)	28004	27642
NORMAL STRESS ON THE RAKE FACE σ_t (psi)	76007	74475
SHEAR STRESS ON THE RAKE FACE τ_t (psi)	26603	26066
SHEAR ANGLE ϕ (degrees)	19.60	19.25
ANGLE θ (degrees)	66.56	66.26
VELOCITY DISCONTINUITY V^* (ipm)	2347.23	2125.62
VELOCITY OF THE CHIP V_c (ipm)	1076.38	773.23

TABLE 5: THEORETICAL RESULTS FOR THE TWO THEORIES.

RAKE ANGLE=-20° FRICTION COEFFICIENT=0.39

BOREHOLE PRESSURE=10000 psi VELOCITY OF THE CUTTER=140 fpm

	COMPRESSIBLE	INCOMPRESSIBLE
TANGENTIAL FORCE PER UNIT AREA F_t/t (psi)	132228	130842
NORMAL FORCE PER UNIT AREA F_n/t (psi)	129923	129009
NORMAL STRESS ON THE SHEAR PLANE σ_n (psi)	68965	66831
SHEAR STRESS ON THE SHEAR PLANE τ_n (psi)	27450	26966
NORMAL STRESS ON THE RAKE FACE σ_t (psi)	69410	67565
SHEAR STRESS ON THE RAKE FACE τ_t (psi)	27070	26349
SHEAR ANGLE ϕ (degrees)	20.54	20.02
ANGLE θ (degrees)	65.04	64.62
VELOCITY DISCONTINUITY V^* (ipm)	2288.21	2061.42
VELOCITY OF THE CHIP V_c (ipm)	1081.82	750.99

TABLE 6: THEORETICAL RESULTS FOR THE TWO THEORIES.

RAKE ANGLE=-15° FRICTION COEFFICIENT=0.42

BOREHOLE PRESSURE=10000 psi VELOCITY OF CUTTER=140 fpm

	COMPRESSIBLE	INCOMPRESSIBLE
TANGENTIAL FORCE PER UNIT AREA F_t/t (psi)	120278	118560
NORMAL FORCE PER UNIT AREA F_n/t (psi)	106538	105573
NORMAL STRESS ON THE SHEAR PLANE σ_n (psi)	62591	60150
SHEAR STRESS ON THE SHEAR PLANE τ_n (psi)	26714	26062
NORMAL STRESS ON THE RAKE FACE σ_t (psi)	62958	60850
SHEAR STRESS ON THE RAKE FACE τ_t (psi)	26442	25556
SHEAR ANGLE ϕ (degrees)	21.54	20.86
ANGLE θ (degrees)	63.07	62.54
VELOCITY DISCONTINUITY V^* (ipm)	2239.70	2002.20
VELOCITY OF THE CHIP V_c (ipm)	1108.90	737.95

TABLE 7 : THEORETICAL RESULTS FOR THE TWO THEORIES

RAKE ANGLE=-25° FRICTION COEFFICIENT=0.38

BOREHOLE PRESSURE=10000 psi VELOCITY OF THE CUTTER=350 fpm

	COMPRESSIBLE	INCOMPRESSIBLE
TANGENTIAL FORCE PER UNIT AREA F_t/t (psi)	158838	157510
NORMAL FORCE PER UNIT AREA F_n/t (psi)	178913	177747
NORMAL STRESS ON THE SHEAR PLANE σ_n (psi)	83196	81534
SHEAR STRESS ON THE SHEAR PLANE τ_n (psi)	30005	29653
NORMAL STRESS ON THE RAKE FACE σ_t (psi)	82009	80546
SHEAR STRESS ON THE RAKE FACE τ_t (psi)	31163	30606
SHEAR ANGLE ϕ (degrees)	19.31	19.03
ANGLE ϑ (degrees)	68.04	67.49
VELOCITY DISCONTINUITY V^* (ipm)	5705.45	5294.30
VELOCITY OF THE CHIP V_c (ipm)	2475.03	1904.70

TABLE 8 : THEORETICAL RESULTS FOR THE TWO THEORIES

RAKE ANGLE=-20° FRICTION COEFFICIENT=0.41

BOREHOLE PRESSURE=10000 psi VELOCITY OF THE CUTTER=350 fpm

	COMPRESSIBLE	INCOMPRESSIBLE
TANGENTIAL FORCE PER UNIT AREA F_t/t (psi)	144164	142598
NORMAL FORCE PER UNIT AREA F_n/t (psi)	145952	144817
NORMAL STRESS ON THE SHEAR PLANE σ_n (psi)	75466	73293
SHEAR STRESS ON THE SHEAR PLANE τ_n (psi)	29384	28895
NORMAL STRESS ON THE RAKE FACE σ_t (psi)	74233	72369
SHEAR STRESS ON THE RAKE FACE τ_t (psi)	30435	29671
SHEAR ANGLE ϕ (degrees)	20.47	20.02
ANGLE θ (degrees)	65.83	65.46
VELOCITY DISCONTINUITY V^* (ipm)	5610.68	5153.54
VELOCITY OF THE CHIP V_c (ipm)	2551.40	1877.50

TABLE 9: THEORETICAL RESULTS FOR THE TWO THEORIES.

RAKE ANGLE=-15° FRICTION COEFFICIENT=0.44

BOREHOLE PRESSURE=10000 psi VELOCITY OF THE CUTTER=350 fpm

	COMPRESSIBLE	INCOMPRESSIBLE
TANGENTIAL FORCE PER UNIT AREA F_t/t (psi)	131152	129322
NORMAL FORCE PER UNIT AREA F_n/t (psi)	119451	118318
NORMAL STRESS ON THE SHEAR PLANE σ_n (psi)	68602	66189
SHEAR STRESS ON THE SHEAR PLANE τ_n (psi)	28693	28071
NORMAL STRESS ON THE RAKE FACE σ_t (psi)	67344	65287
SHEAR STRESS ON THE RAKE FACE τ_t (psi)	29631	28726
SHEAR ANGLE ϕ (degrees)	21.58	20.99
ANGLE θ (degrees)	63.90	63.45
VELOCITY DISCONTINUITY V^* (ipm)	5500.80	5014.51
VELOCITY OF THE CHIP V_c (ipm)	2627.80	1860.32

TABLE 10 : THEORETICAL RESULTS FOR DIFFERENT VALUES OF BOREHOLE PRESSURE.
RAKE ANGLE=-15° FRICTION COEFFICIENT=0.42 PORE PRESSURE=0 psi
VELOCITY OF THE CUTTER=140 fpm

	σ_b =10000 psi	σ_b =5000 psi	σ_b =2000 psi
TANGENTIAL FORCE PER UNIT AREA F_t/t (psi)	120278	108900	99119
NORMAL FORCE PER UNIT AREA F_n/t (psi)	106538	91253	79725
NORMAL STRESS ON THE SHEAR PLANE σ_n (psi)	62591	47115	35098
SHEAR STRESS ON THE SHEAR PLANE τ_n (psi)	26714	24333	21572
NORMAL STRESS ON THE RAKE FACE σ_t (psi)	62957	51171	41471
SHEAR STRESS ON THE RAKE FACE τ_t (psi)	26442	21491	17418
SHEAR ANGLE ϕ (degrees)	21.54	20.01	18.09
ANGLE θ (degrees)	63.07	60.02	56.93
VELOCITY DISCONTINUITY V^* (ipm)	2239.70	2337.70	2454.20
VELOCITY OF THE CHIP V_c (ipm)	1108.90	1247.90	1406.40

TABLE 11 : THEORETICAL RESULTS FOR DIFFERENT VALUES OF PORE PRESSURE.

RAKE ANGLE=-15 FRICTION COEFFICIENT=0.42 BOREHOLE PRESSURE=10000 psi

VELOCITY OF THE CUTTER=140 fpm

	$\sigma_{p1}=\sigma_{p2}=0$ psi	$\sigma_{p1}=\sigma_{p2}=5000$ psi	$\sigma_{p1}=\sigma_{p2}=10000$ psi
TANGENTIAL FORCE PER UNIT AREA F_t/t (psi)	120278	114961	106478
NORMAL FORCE PER UNIT AREA F_n/t (psi)	106538	95998	82541
NORMAL STRESS ON THE SHEAR PLANE σ_n (psi)	62591	56514	47066
SHEAR STRESS ON THE SHEAR PLANE τ_n (psi)	26714	25122	22088
NORMAL STRESS ON THE RAKE FACE σ_t (psi)	62957	58374	50564
SHEAR STRESS ON THE RAKE FACE τ_t (psi)	26442	23799	19800
SHEAR ANGLE ϕ (degrees)	21.54	20.43	18.19
ANGLE θ (degrees)	63.07	61.63	59.24
VELOCITY DISCONTINUITY V^* (ipm)	2239.70	2300.39	2418.98
VELOCITY OF THE CHIP V_c (ipm)	1108.90	1195.67	1359.09

APPENDIX IV

Mohr's Envelopes

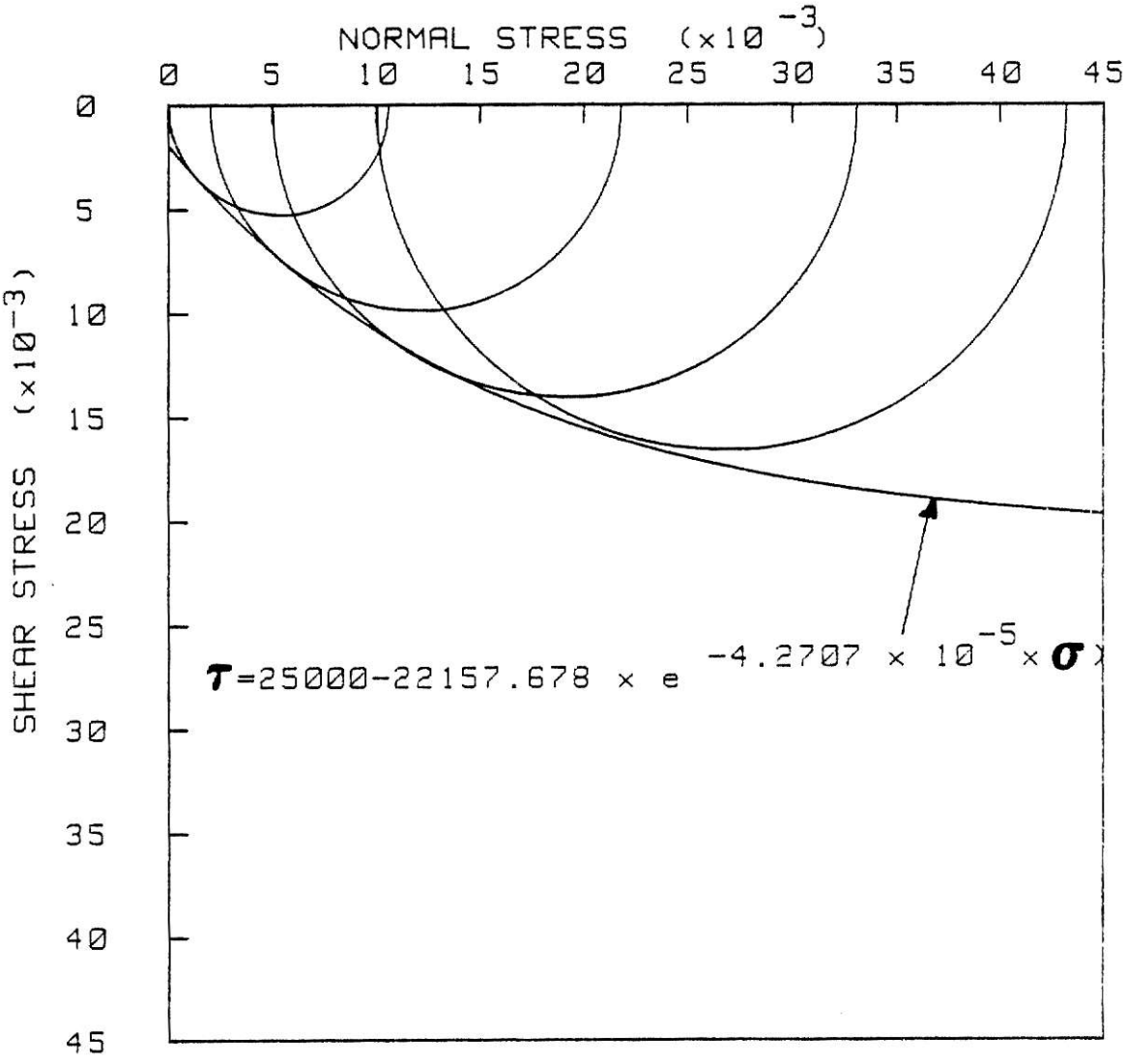

FIGURE 30 : MOHR'S ENVELOPE FOR CHEATHAM'S DATA

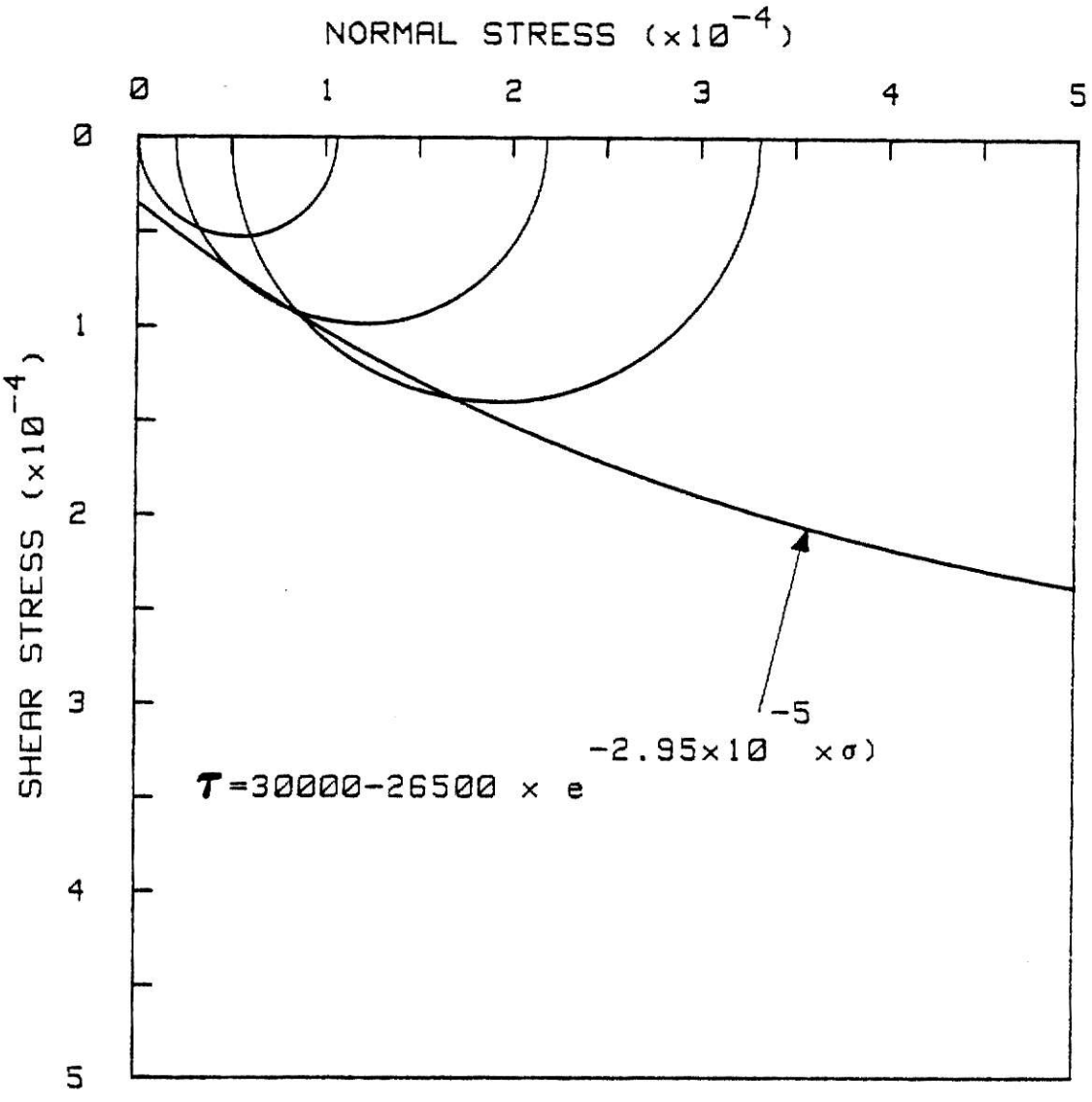

FIGURE 31 : MOHR'S ENVELOPE FOR MELAUGH'S DATA.

ACKNOWLEDGEMENTS

I wish to express my sincere appreciation and gratitude to Dr. Frederic C. Appl, Professor of Mechanical Engineering for his guidance and counsel throughout this work.

My thanks are due to the Department of Mechanical Engineering and Christensen Diamond Products Inc. for their financial support during my graduate study.

I am grateful to Dr. C.L.D. Huang, Professor of Mechanical Engineering for serving on my committee and for frequent encouragement for academic work.

My thanks are also due to Dr. K.K. Hu, Associate Professor of Civil Engineering for serving as a graduate committee member.

Finally my thanks are due to my family whose support and inspiration has helped me throughout my graduate study.

VITA

VEERAMANI PRAKASH

Candidate for the Degree

Master of Science

THESIS: ROCK CUTTING THEORY FOR PDC CUTTERS

MAJOR FIELD: Mechanical Engineering

BIOGRAPHICAL:

Personal Data:	Born October 5, 1958 at Madras, India, the son of K. Veeramani and K. Narayani.
Education:	Graduated from Vidya Mandir Matriculation School, Madras, India in 1974; recieved a B.E(HONORS) degree in Mechanical Engineering from Madras University in July 1980, completed requirements for the M.S degree in June 1982.
Experience:	July, 1980 to December, 1980 served as a Production Engineer in Unity Forgings, Madras India; January, 1981 to June, 1982 served as Graduate Research Assistant in the Mechanical Engineering Department, Kansas State University.

ROCK CUTTING THEORY FOR PDC CUTTERS

by

VEERAMANI PRAKASH
B.E(HONORS)., Madras University, India, 1980

AN ABSTRACT OF A MASTER'S THESIS

submitted in partial fulfillment of the
requirements for the degree

MASTER OF SCIENCE

Department of Mechanical Engineering

Kansas State University
Manhattan, Kansas

1982

ABSTRACT

A rock cutting theory for PDC cutters is developed as a first step in developing a drilling theory for oil well drill bits. The cutting problem is solved by two different plasticity theories and the solutions are compared. The solutions are also compared to experimental work. The cutting forces calculated from the theory agree fairly well with the experimental results. The velocity effect in the theory partially explains the differences in the experimental results obtained previously by two different investigators.